



Marianne Liebi- Material Science at Large Scale Facilities

Coherent Diffraction Imaging

EPFL Master Course 2024 MSE435



| 09.09.24 | Introduction, sources, beamlines, detectors | Steven Van Petegem |
|----------|---|-------------------------------------|
| 16.09.24 | Holiday | |
| 23.09.24 | Excursion to PSI | Steven Van Petegem / Marianne Liebi |
| 30.09.24 | Interaction with matter | Steven Van Petegem |
| 07.10.24 | Fluorescence | Marianne Liebi |
| 14.10.24 | Diffraction I | Steven Van Petegem |
| 21.10.24 | Break | |
| 28.10.24 | Small angle x-ray scattering | Marianne Liebi |
| 04.11.24 | Cancelled | |
| 11.11.24 | XANES/EXAFS | Marianne Liebi |
| 18.11.24 | Phase contrast / Tomography | Steven Van Petegem |
| 25.11.24 | Coherent imaging | Marianne Liebi |
| 02.12.24 | Diffraction II / Neutron imaging | Steven Van Petegem |
| 09.12.24 | PEEM / Magnetic scattering | Steven Van Petegem |
| 16.12.24 | Case study presentations | Steven Van Petegem / Marianne Liebi |



 Question: Do you get the same information if you measure at a K-edge or an L-edge of a material?

The question is not simple but the fast answer is that the information one can get from K and L edges XANES is complimentary.

K- and L1 edges XANES mainly probe the p-density of unoccupied states because there s to d transition are formally forbidden. Nevertheless the K pre-edges correspond to s to d forbidden transitions providing information about 3d elements local symmetry, intense pre-edge correspond to non-centrosymmetric coordination (e.g. tetrahedral).

L2 and L3 are sensitive to d-projected density of unoccupied states.

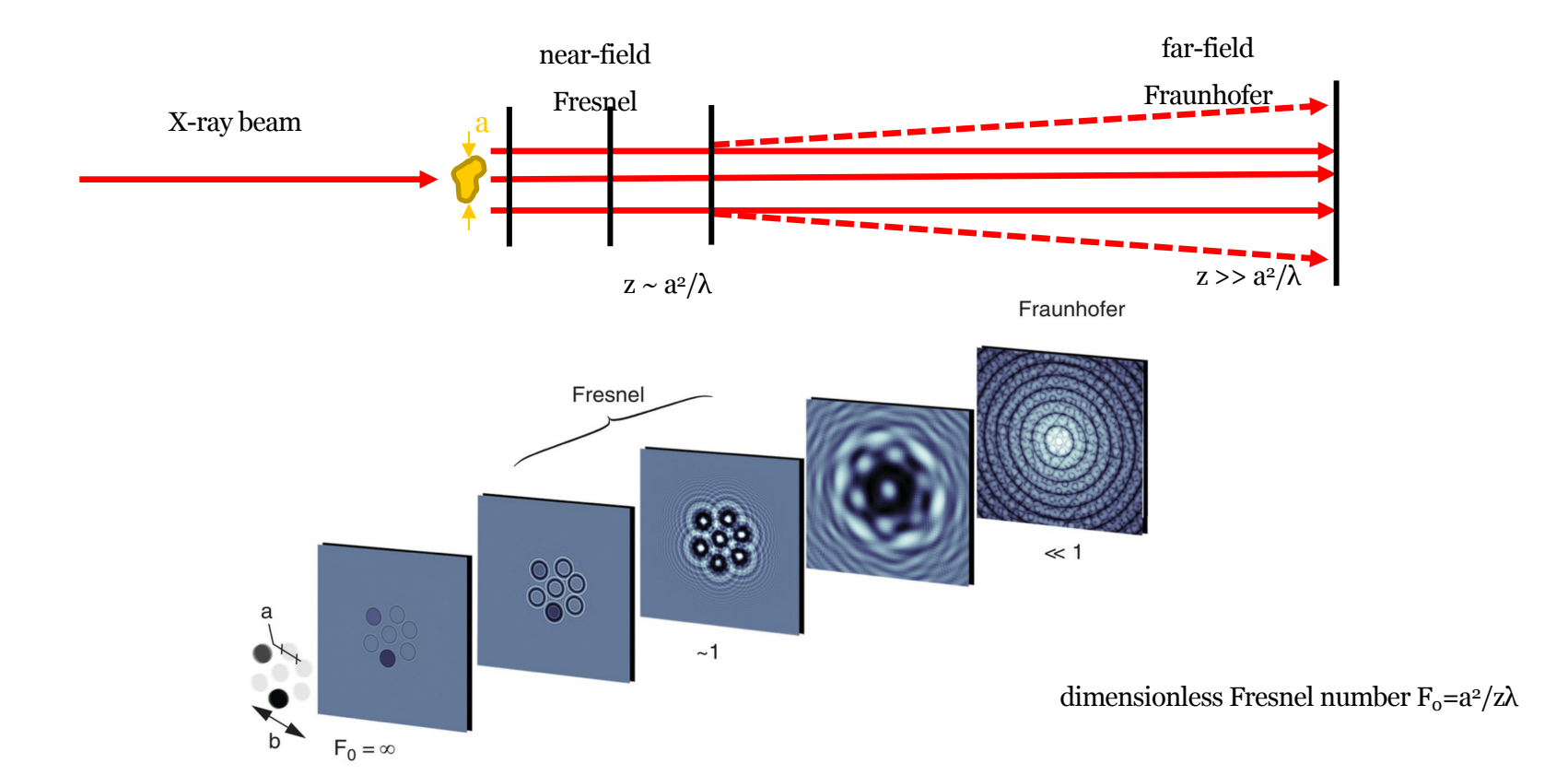
K-edges of heavy elements are also often very broad due to high lifetime broadening, therefore they may not show many features except for the E-shift due to the oxidation state. L-edges are more narrow showing more fine structure, which helps to distinguish fine details of the local structure.

For EXAFS K-edges are preferable, as they are better separated in energy, less overlap with other elements, easier to measure up to high wavenumbers with good statistics.

Olga Safonova (Beamline Scientist SuperXAS)

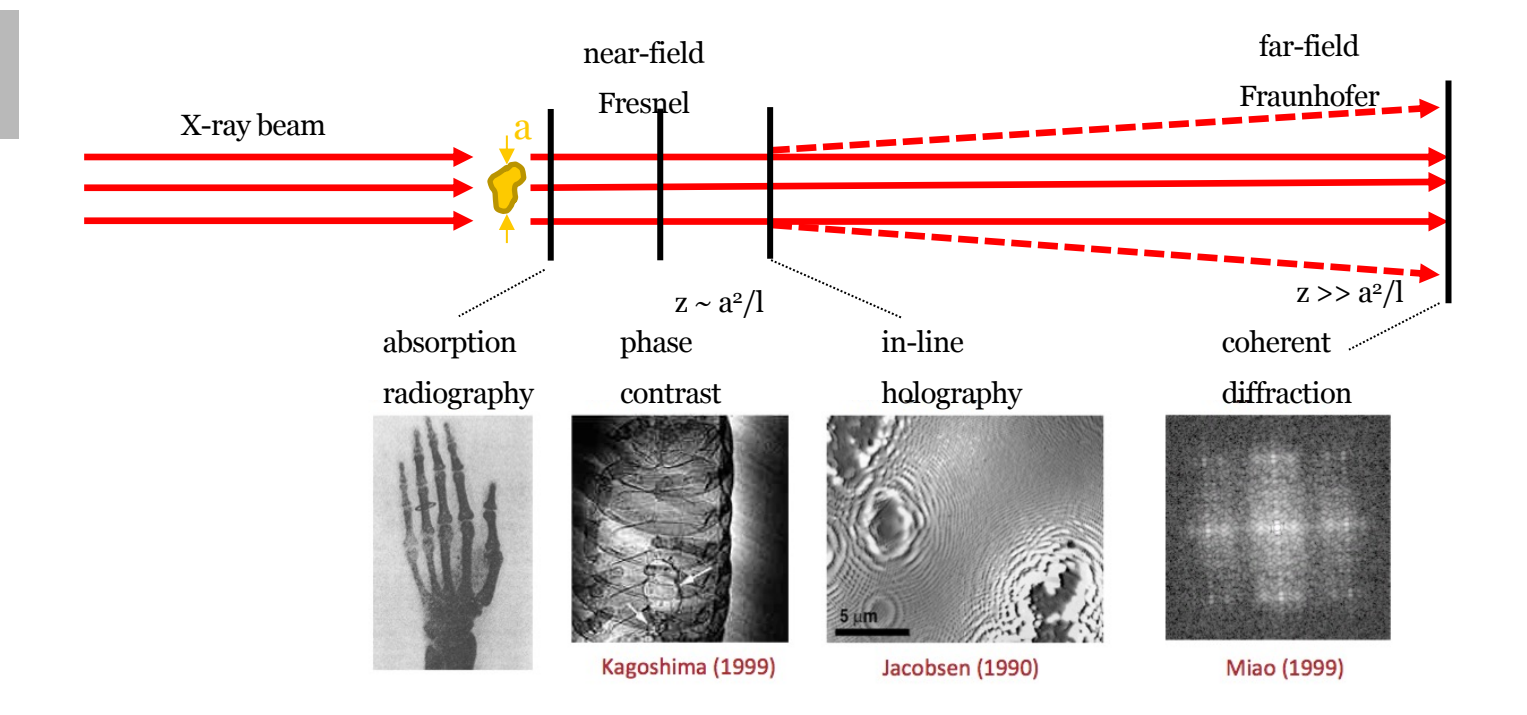


Far-field Fraunhofer Regim





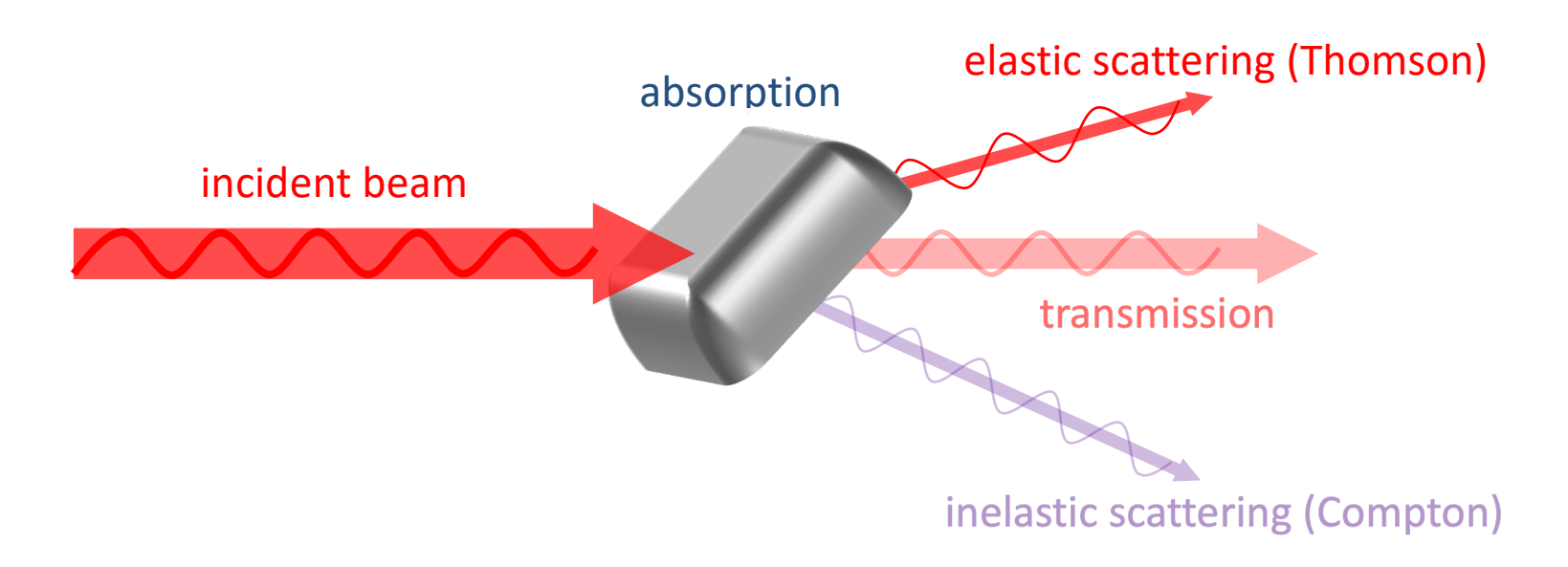
X-ray imaging: full-field





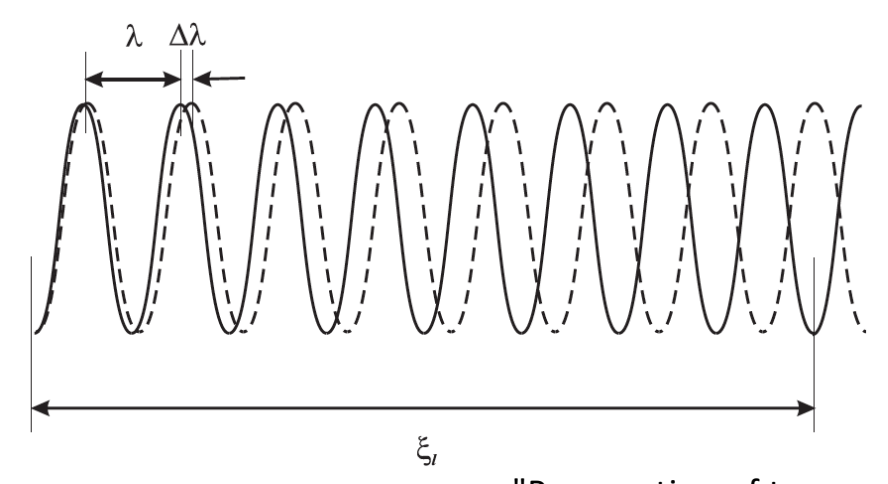
Interaction of X-rays with matter

interaction with electrons





Longitudinal coherence

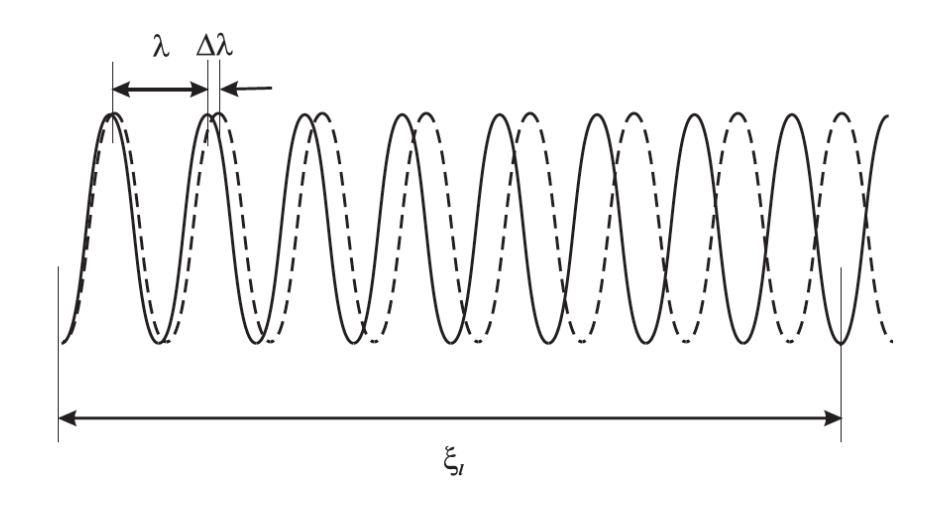


Longitudinal coherence length: $\xi_{\rm l} \simeq \frac{1}{2} \frac{\lambda^2}{\Delta \lambda}$

"Propagation of two waves with wavelengths I and I + DI. The longitudinal coherence length is defined as the distance over which the phase difference between the two waves is p."



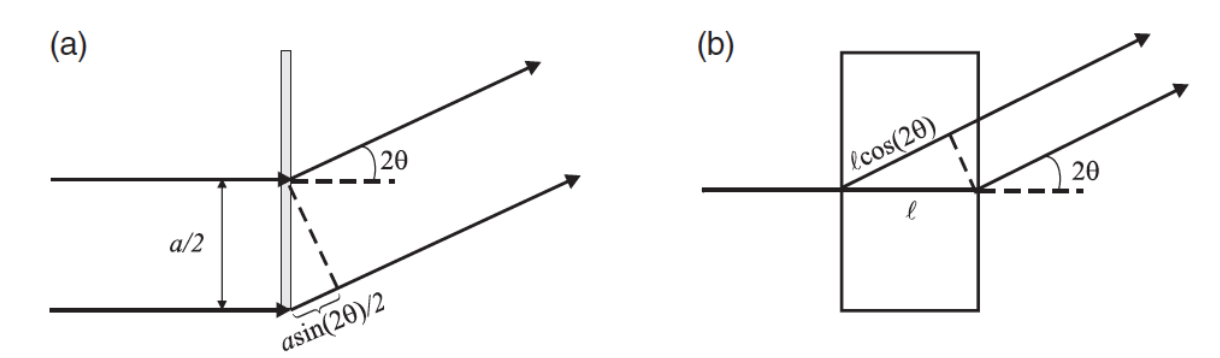
Longitudinal coherence



Longitudinal coherence length:
$$\xi_{\rm l} \simeq \frac{1}{2} \frac{\lambda^2}{\Delta \lambda}$$
 Si (111) monochromator: DI/I = 1.3×10⁻⁴ I = 2 Å \rightarrow x_l \approx 800 nm



Implications of longitudinal coherence

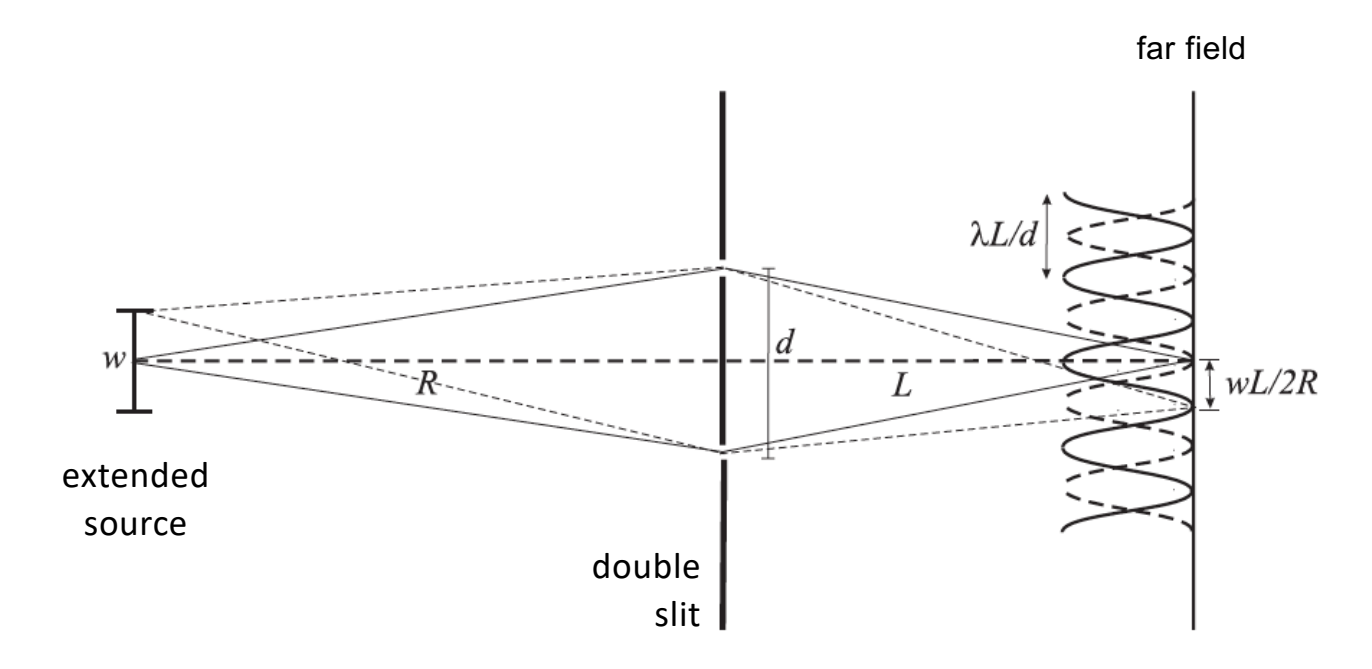


A condition for coherence is that the path length difference between points scattered from different points at the sample is smaller than the longitudinal coherence length \mathbf{x}_{l}

$$\frac{\Delta\lambda}{\lambda} < \frac{s}{a}$$
 In order to resolve an object of size a = 5 µm to within s = 10 nm, one has to keep the bandwith below $2x10^{-3} \rightarrow$ crystal monochromator



Transversal coherence



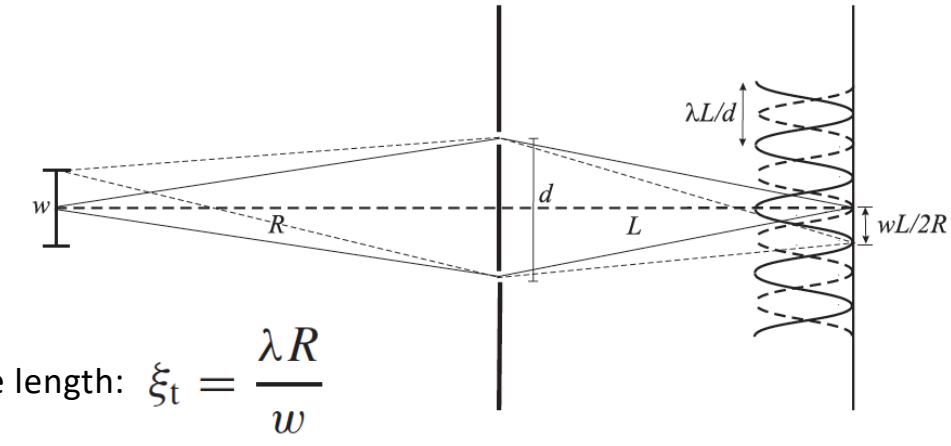
Transversal coherence length:
$$\xi_{\rm t} = \frac{\lambda R}{w}$$

Maximum distance between two slits such that they produce constructive interference when illuminated by an extended source size

J. F. Van der Veen & F. Pfeiffer J. Phys.: Condens. Matter 16, 5003 (2004)



Transversal coherence



Transversal coherence length: $\xi_{\mathrm{t}} = \frac{\lambda R}{w}$

Numbers for a typical 3rd generation source

Laboratory:
$$x_h < 1 \mu m$$

$$R = 34 \text{ m}$$

$$w_v = 20 \text{ mm} \implies x_v = 340 \text{ }\mu\text{m}$$

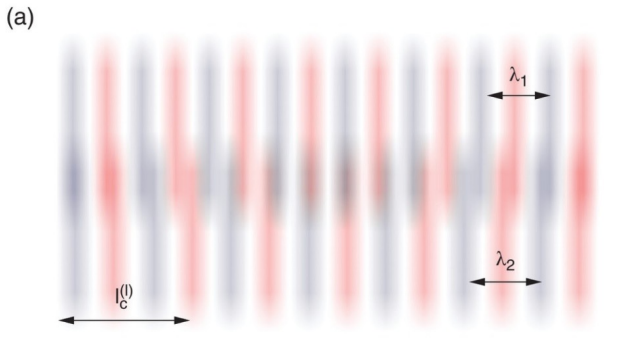
$$w_h = 200 \text{ mm} \implies x_h = 34 \mu \text{m}$$

$$w_{v} = 6 \, \mu \text{m}, R = 60 \, \text{m}, I = 1 \, \text{Å}$$

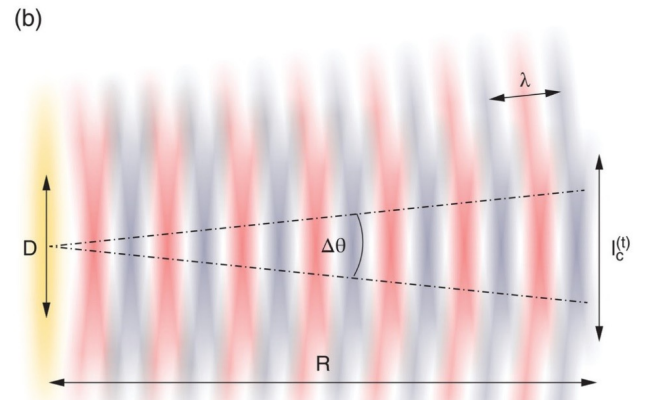
$$x_v \sim 1 \text{ mm}$$



Coherence



longitudinal (temporal) coherence length determined by monochromacy of the source



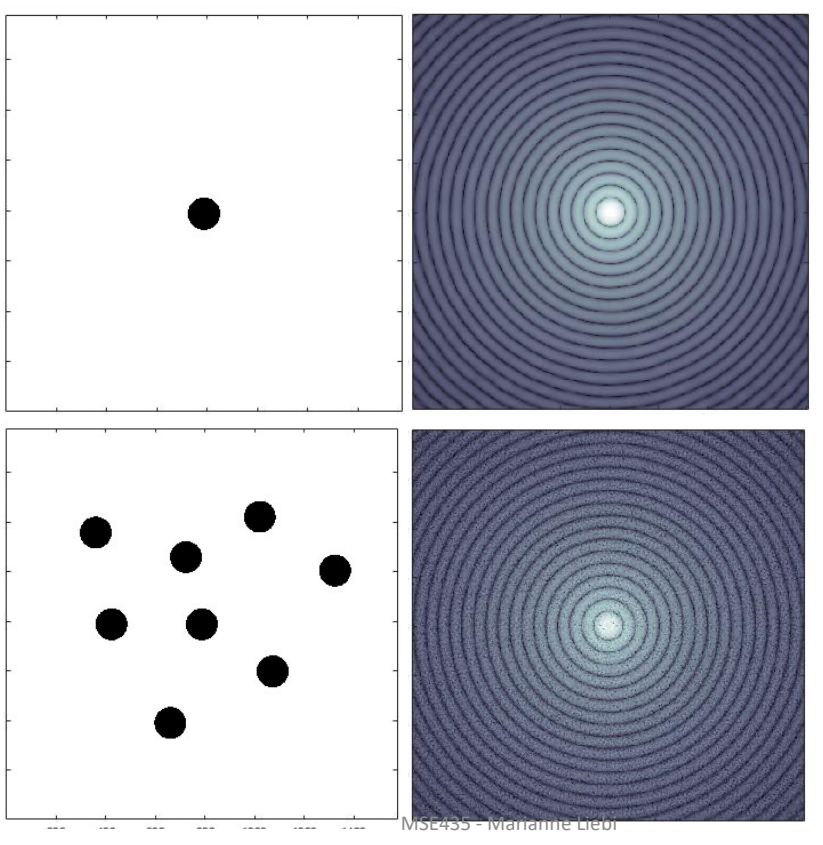
transverse (spatial) coherence length depends on the beam divergence and source size

Willmott, P. (2019). Scattering Techniques. <u>An Introduction to Synchrotron Radiation</u>, <u>John Wiley & Sons</u>, <u>Ltd: 133-221</u>.

TIF 326



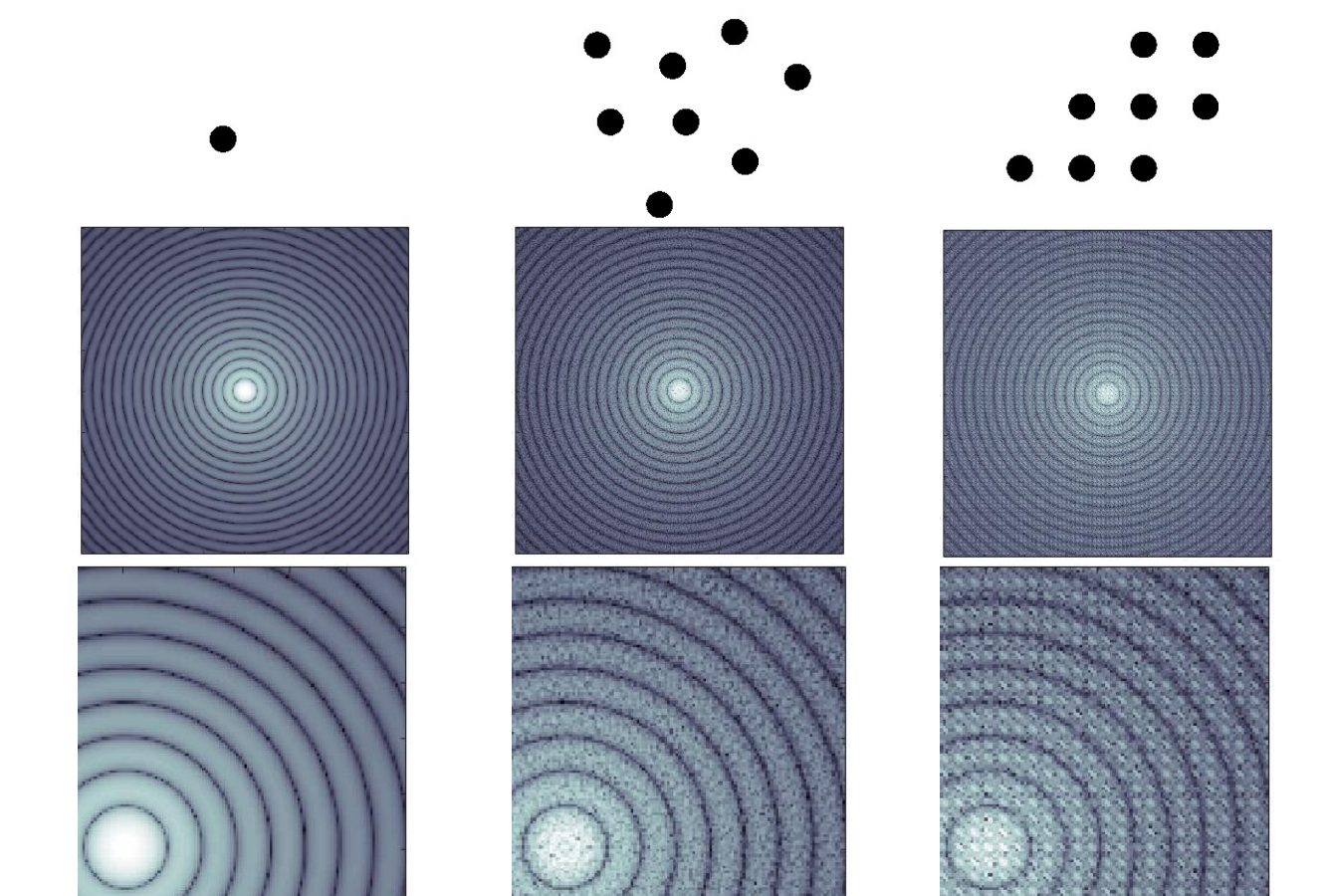
small-angle X-ray scattering



scattering pattern shows average over particle ensemble



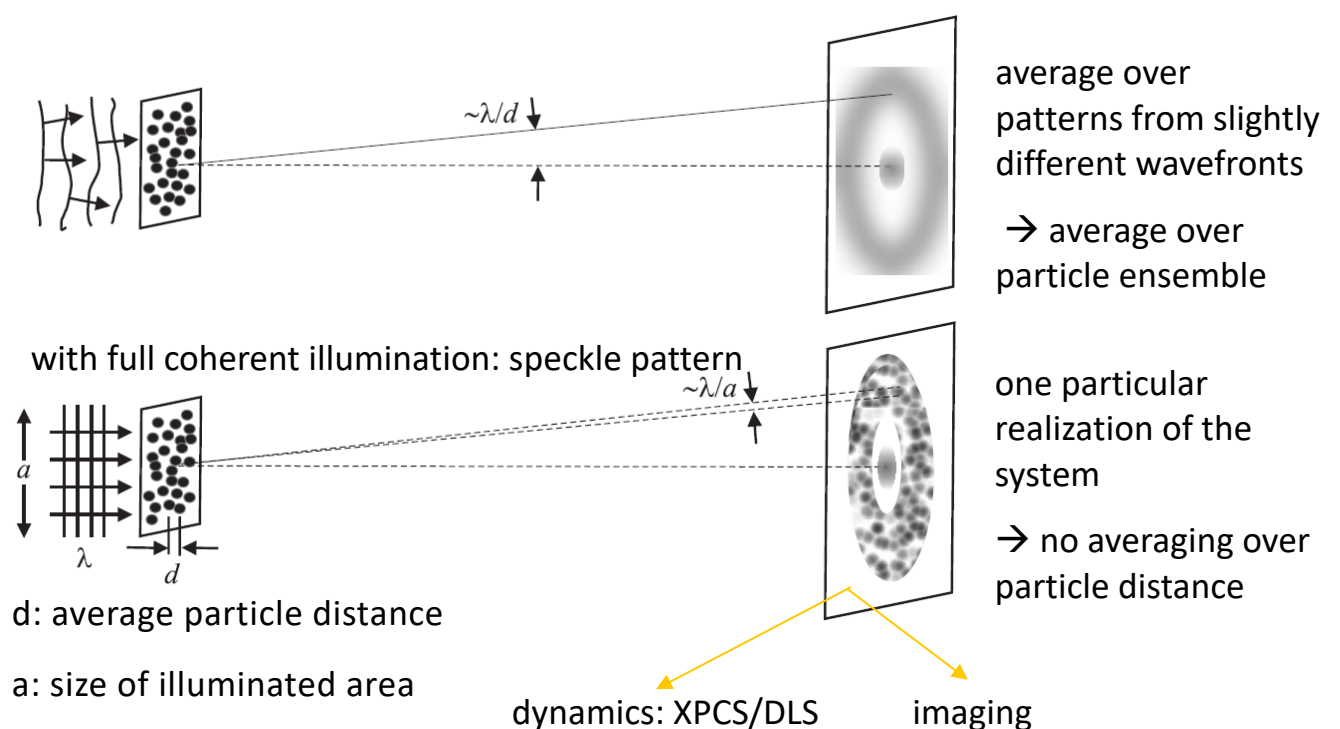
Scattering with coherent illumination





Coherent scattering

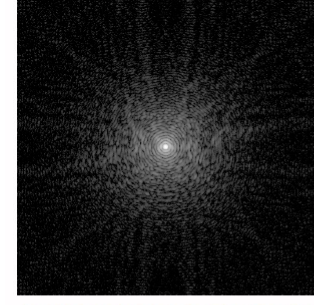
X-ray scattering from a disordered medium in the far field (Fraunhofer)



J. F. Van der Veen & F. Pfeiffer J. Phys.: Condens. Matter 16, 5003 (2004)

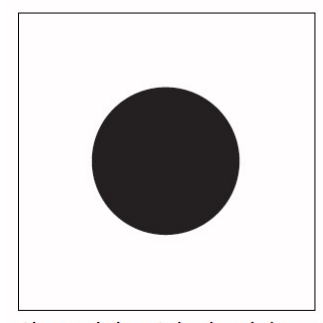


Coherent diffraction imaging (CDI)



Fourier constraint

image is consistent with measured intensity

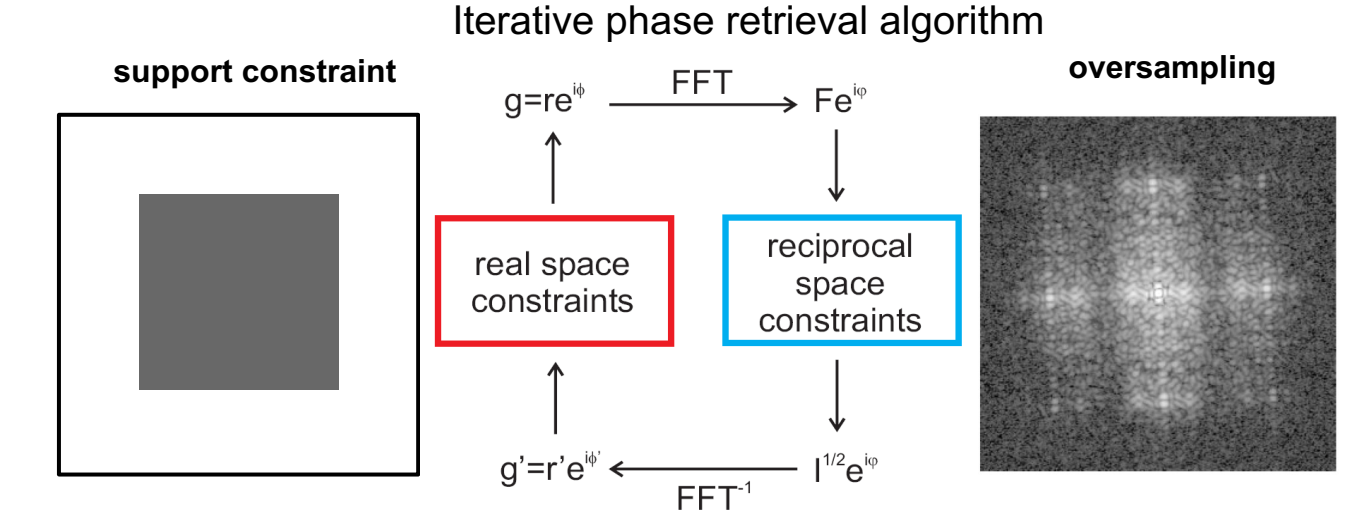


support constraint

the object is inside a finite support



Coherent diffraction imaging (CDI)



J.R. Fienup Appl. Opt. 21 (1982) 2758

Sample consisting of 100 nm Au nanodots

J. Miao et al., Nature **400** (1999) 342



Coherent diffraction imaging (CDI)

J.R. Fienup Appl. Opt. 21 (1982) 2758

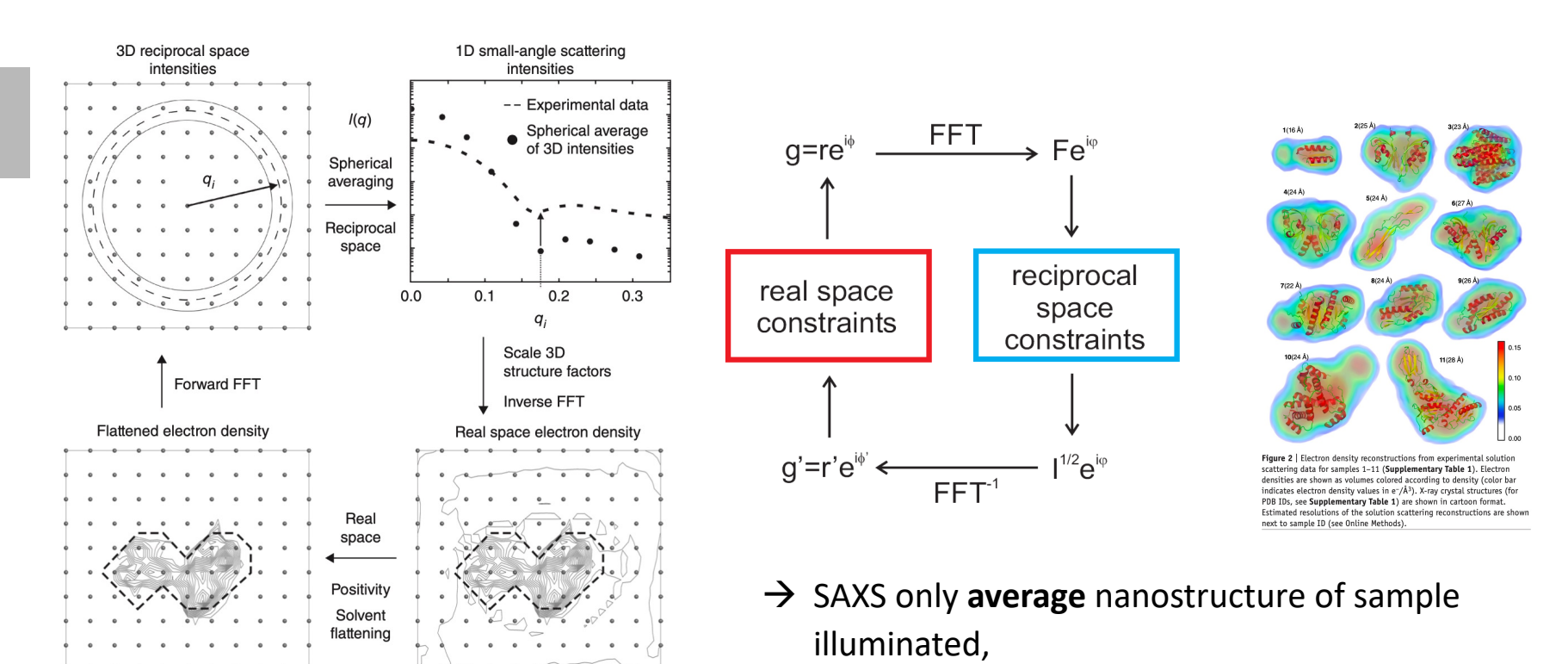
Resolution not limited by optics

Sample consisting of 100 nm Au nanodots

J. Miao et al., Nature **400** (1999) 342



SAXS analysis: iterative approach



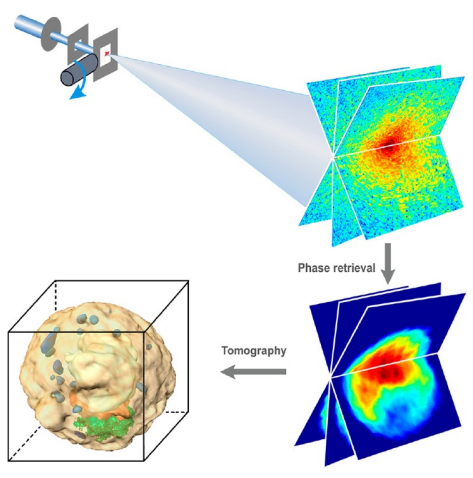
Grant, T. D., Nature Methods 2018, 15, 191.

→ CDI image of the nanostructure illuminated



3D coherent diffraction imaging

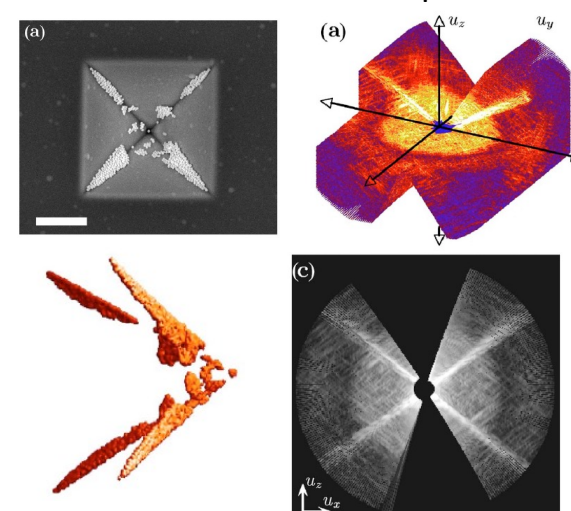
School of J. Miao



H. Jiang *et al.*, PNAS **107** (2010) 11234

- 2D phase retrieval on each 2D coherent diffraction pattern recorded at different angles
- Conventional tomography

School of H. N. Chapman



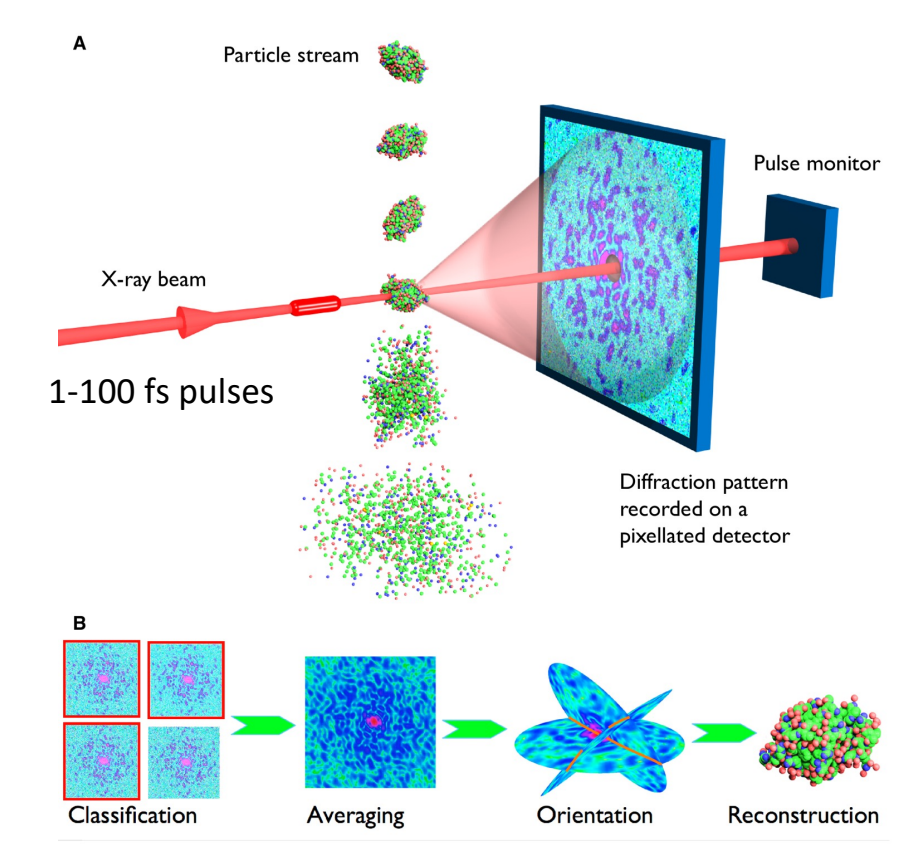
H. N. Chapman *et al.*, J. Opt. Soc. Am. A **23** (2006) 1179

- 3D reciprocal space construction from 2D coherent diffraction patterns recorded at different angles
- 3D phase retrieval



X-ray free electron lasers (X-FELs)

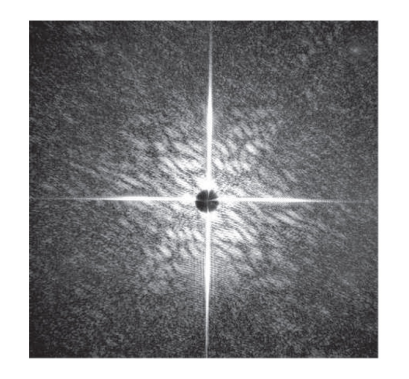
Diffract-before-destroy approach

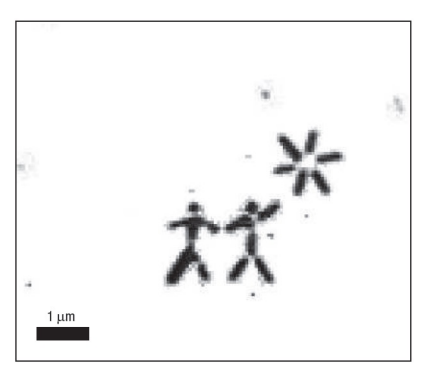


https://cid.cfel.de/research/single_particle_imaging/ Henry Chapman, CFEL. Science, 2007, 316, 1444-48.



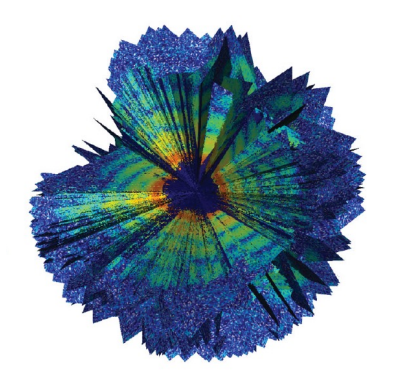
CDI in free electron lasers

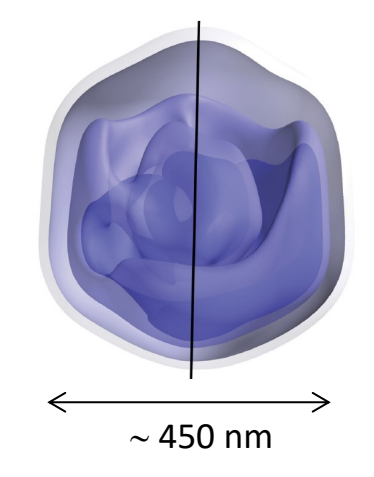




Test sample @ FLASH, λ = 32 nm

H. N. Chapman *et al.*, Nat. Phys. **2** (2006) 839



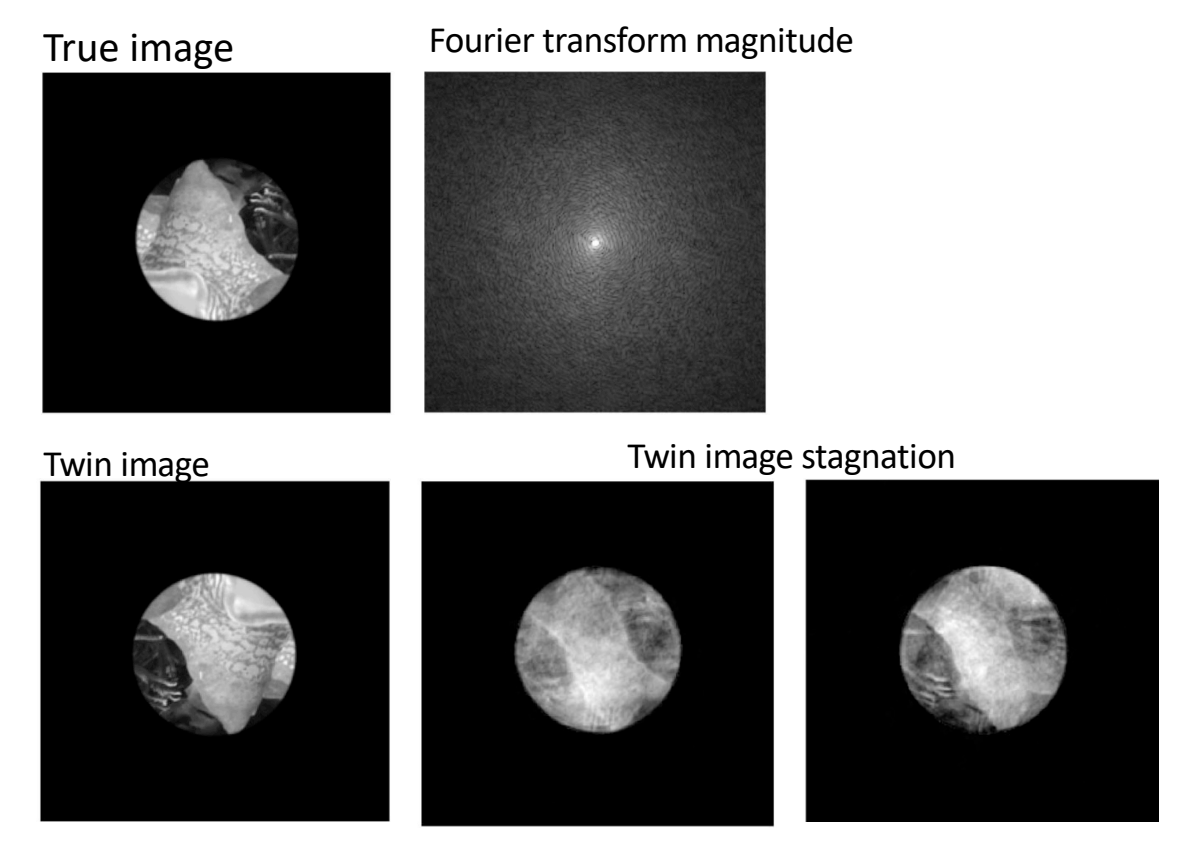


Giant mimivirus particle @ LCLS, free electron laser

T. Ekeberg *et al.*, Phys. Rev. Lett. **114** (2015) 098102



CDI: Twin-image problem



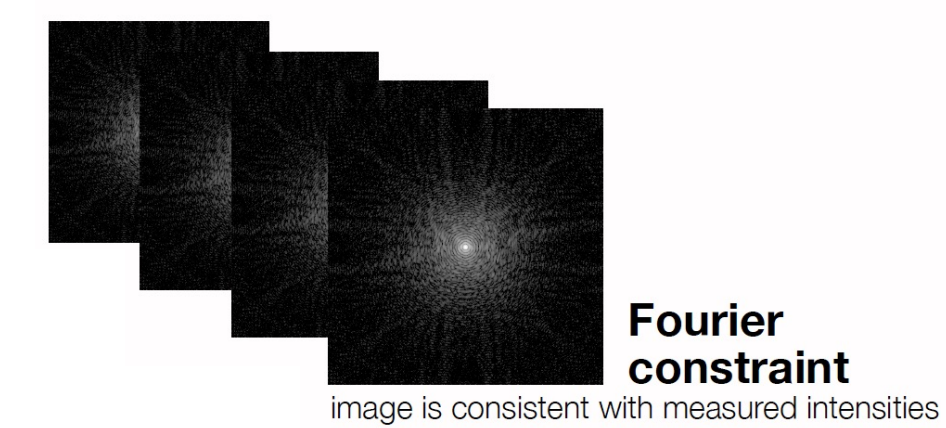
M. Guizar-Sicairos and J. R. Fienup, J. Opt. Soc. Am A 29, 2367 (2012)



- X-ray microscopy with high resolution not limited by X-ray optics
- In Bragg geometry, it is sensitive to atomic displacements
- The convergence of the phase retrieval algorithms requires:
 - Isolated sample in 3D
 - Sample size limited to a few microns
- Practical consequences (mostly in forward direction)
 - Not robust to realistic sample preparation
 - Convergence issues
 - Typically sample lying on a membrane: missing wedge in 3D reciprocal space
 - Beamstop is often required: missing low frequencies
- CDI is done at FELs, Bragg geometry beamlines with micro- or nano-focus (Argonne, ESRF, Petra III, MAX-IV) and a few beamlines in forward direction (ESRF). Permanent setups exist for both soft and hard X-rays.



Ptychography



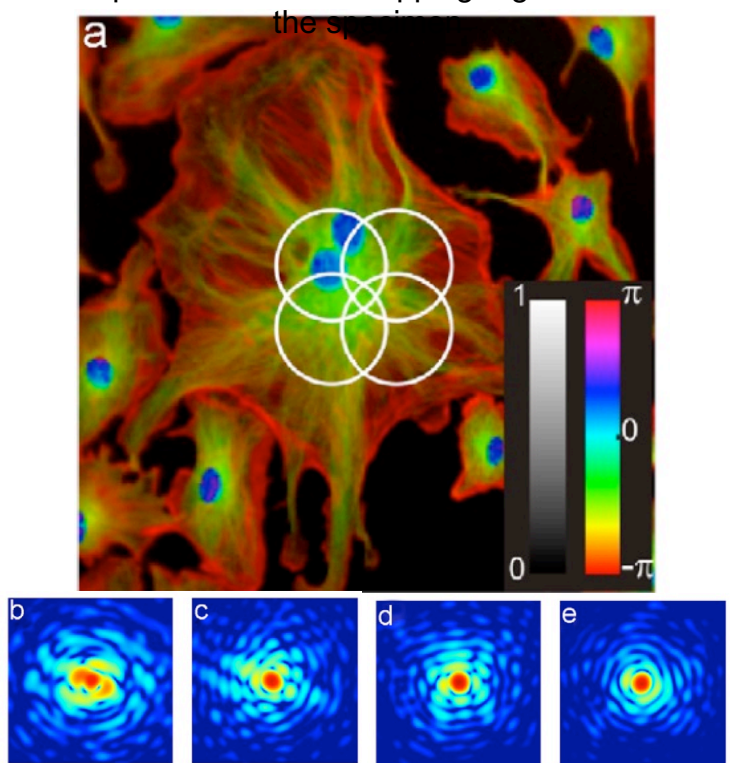
overlap constraint

overlapping regions agree and incident wave field is unique

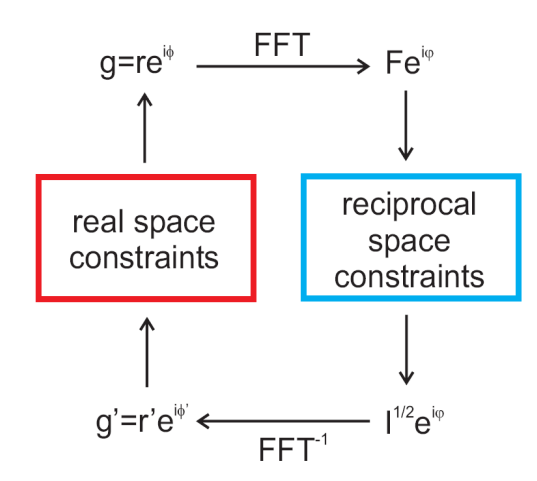


Ptychography

oversampling by coherent diffraction patterns from overlapping regions of



Phase retrieval algorithms to reconstruct complex-valued transmissivity

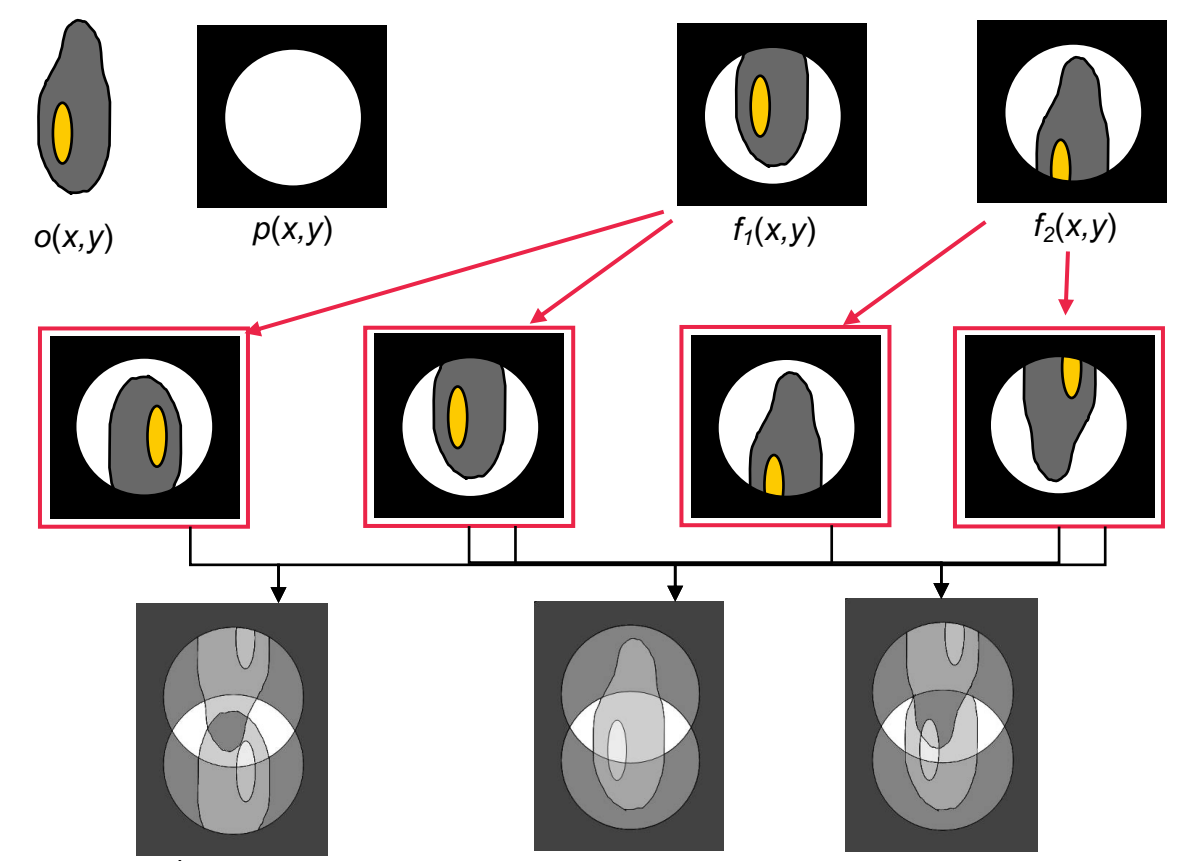


H. M. L. Faulkner & J. M. Rodenburg,

Phys. Rev. Lett. 93 (2004) 023903



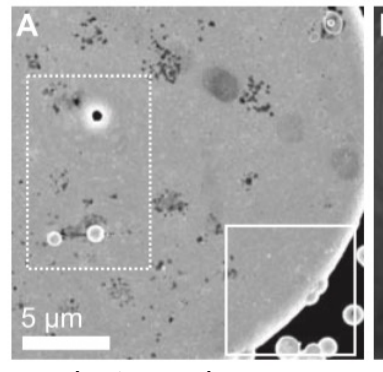
Ptychography: overlap constraint

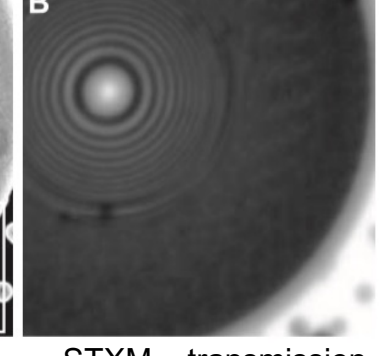


Overlap in ptychography is a crucial constraint for phase retrieval



Ptychography with probe retrieval





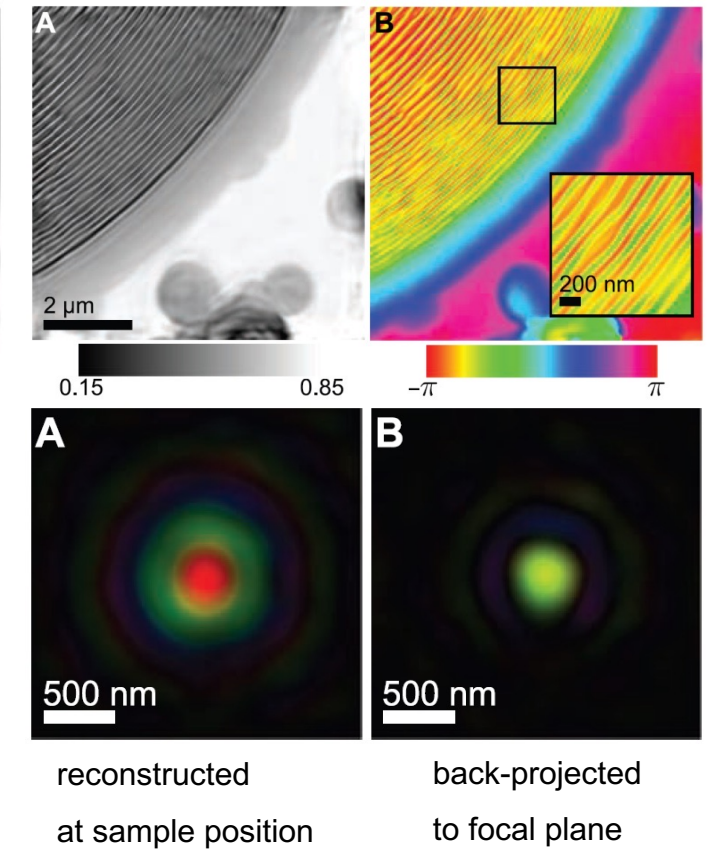
electron microscopy
gold layer on top

STXM – transmission 300 nm probe size

$$\psi_j(\mathbf{r}) = P(\mathbf{r} - \mathbf{r}_j)O(\mathbf{r})$$

Enough information to retrieve complexvalued illumination simultaneously

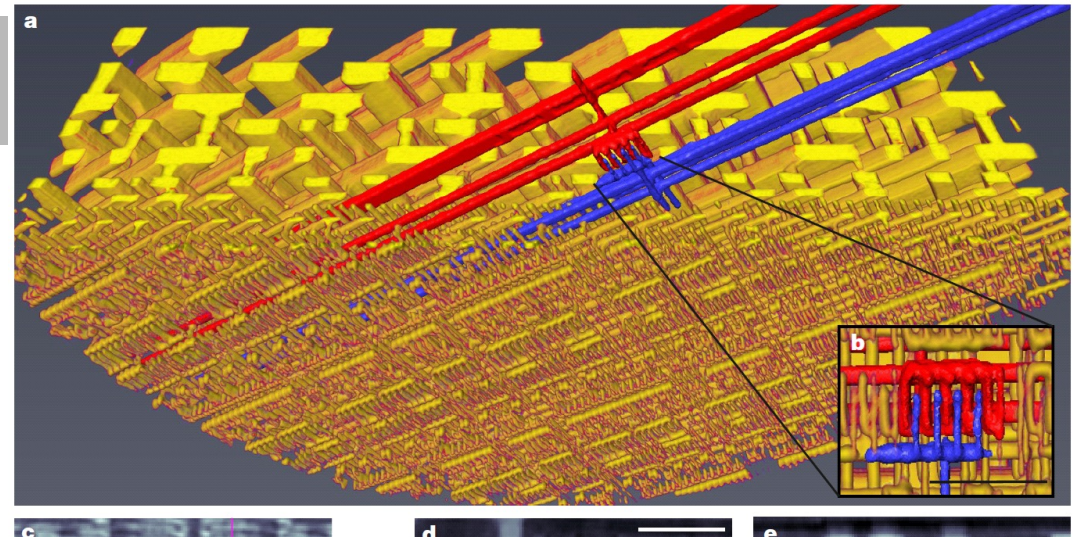
P. Thibault et al., Science 321 (2008) 379





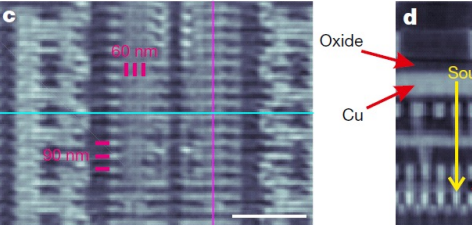
Ptychographic nanotomography

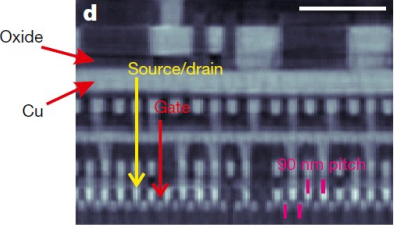
Intel chip, 22 nm technology

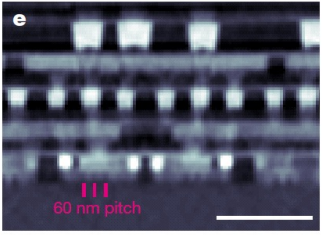


Resolution: new record: 4nm resolution

14.6 nm







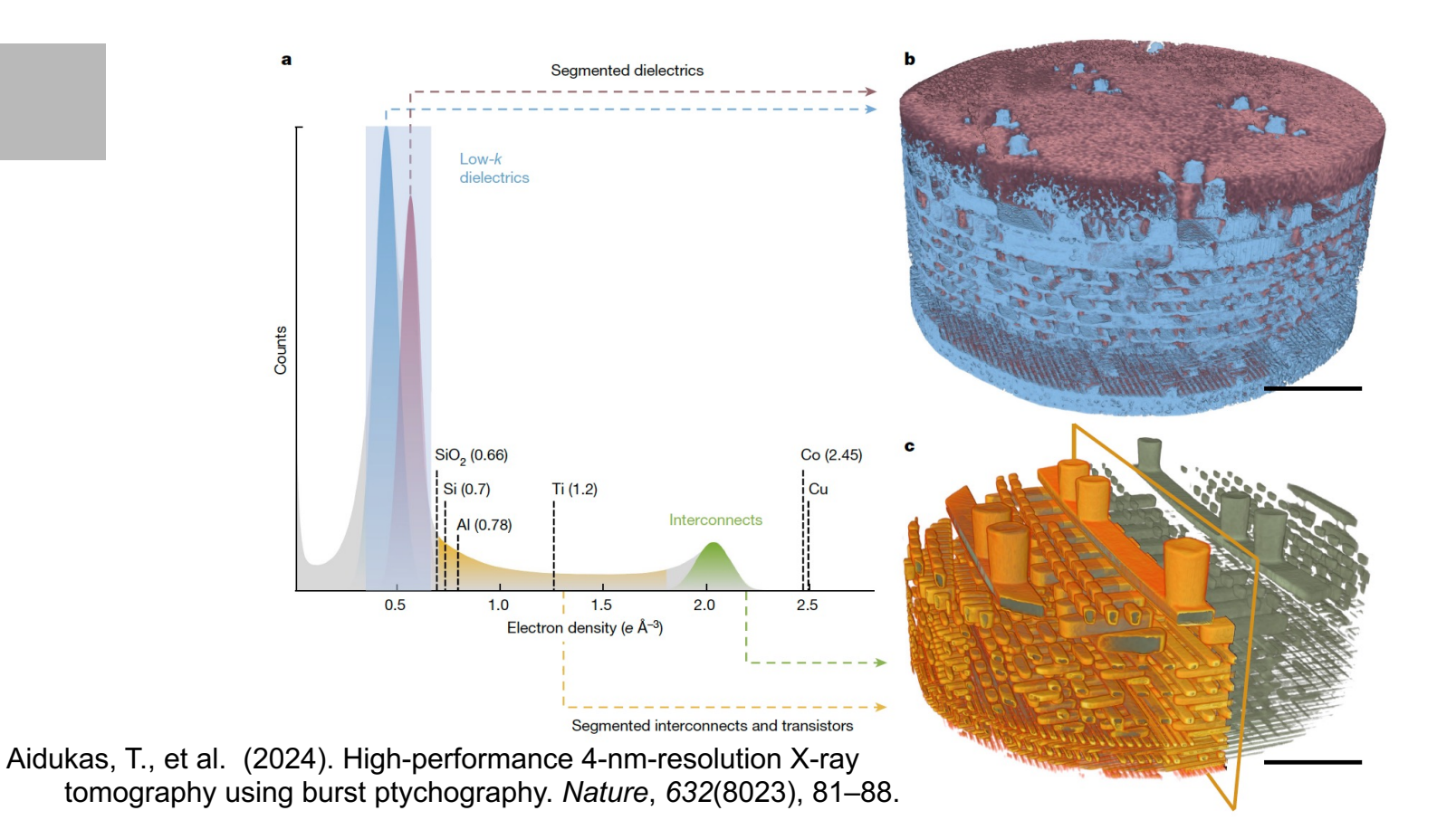
Scale bars:

500 nm

M. Holler *et al.*, Nature **543** (2017) 402

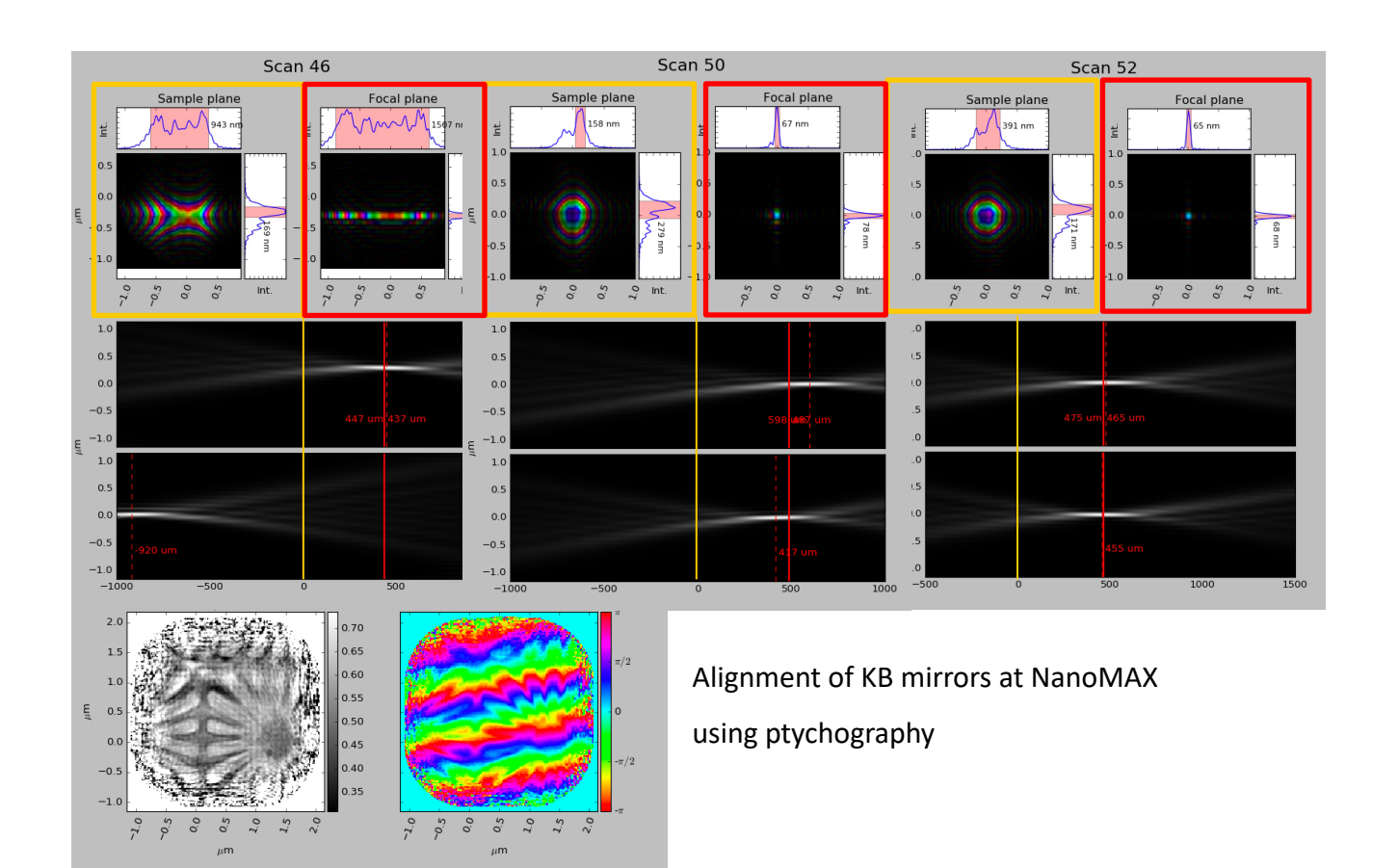


Ptychographic Nanotomography





X-ray optics characterization with ptychography

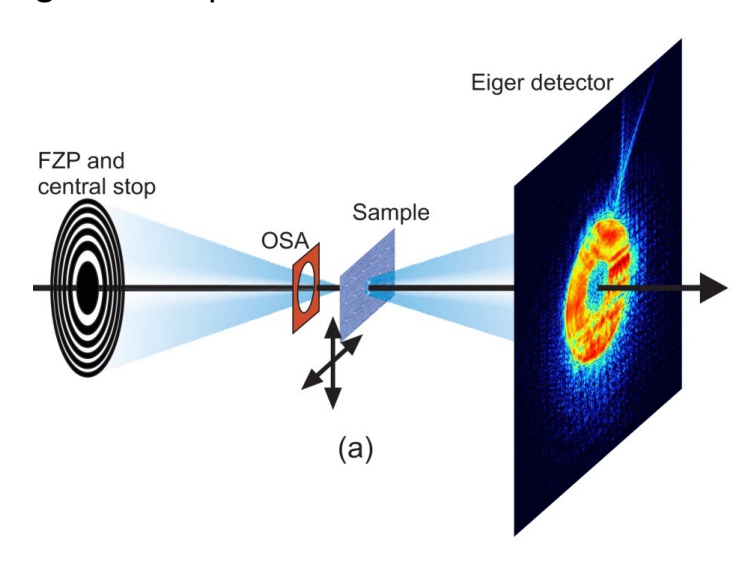


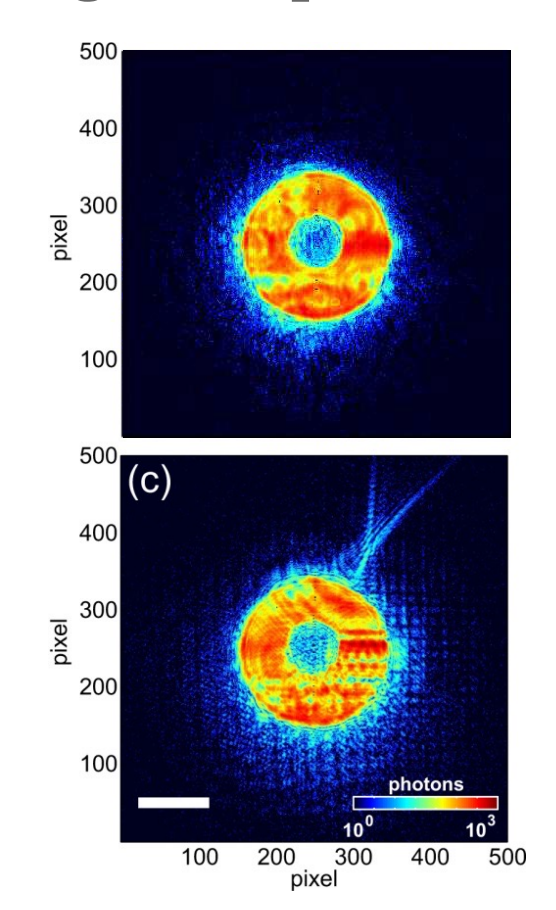


Imaging throughput – The Eiger self portrait

Sample 5 mm downstream of focus Beam at sample ~ 10 microns Scanning average step 3.5 microns

Eiger as sample and detector

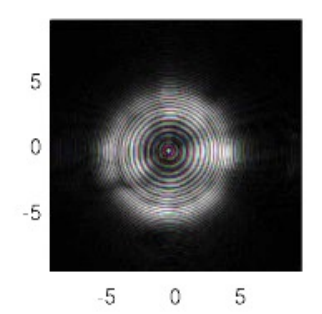


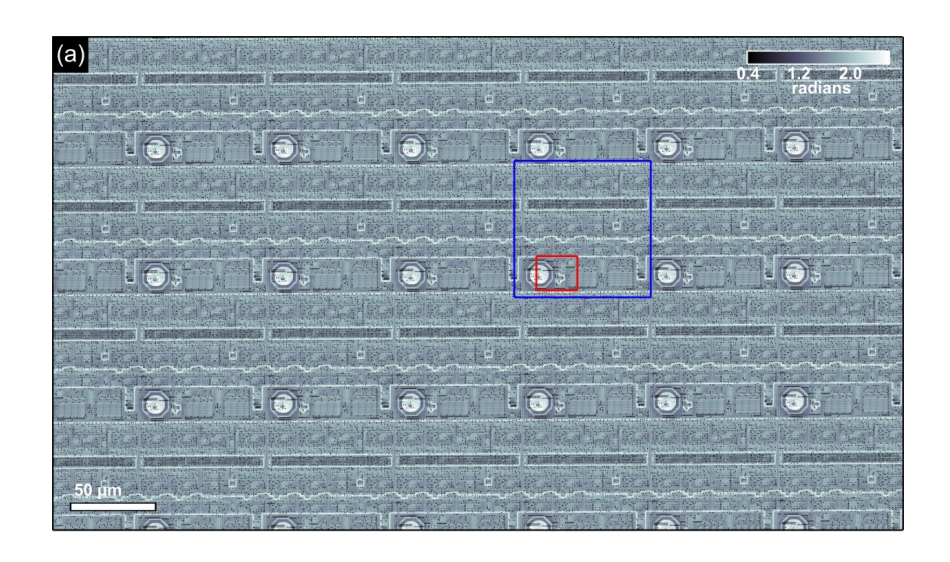


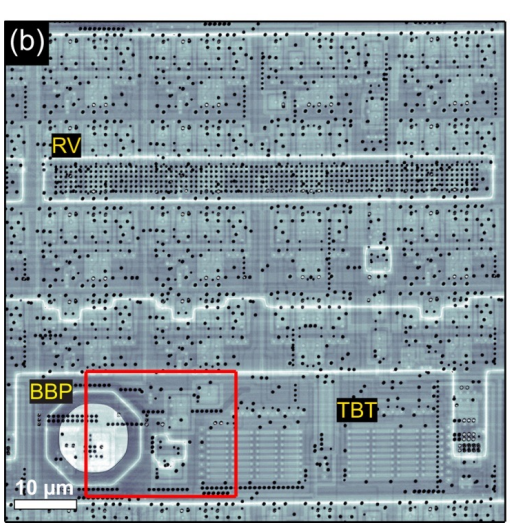


Imaging throughput – The Eiger self portrait

98.4 Mpixel (13,028 x 7,556)
Resolution 41 nm, 38.4 nm pixel
> 25,000 resolution elements / second
40 microsecond per resolution element



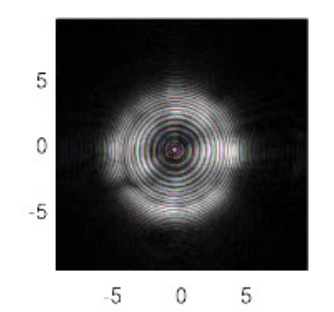


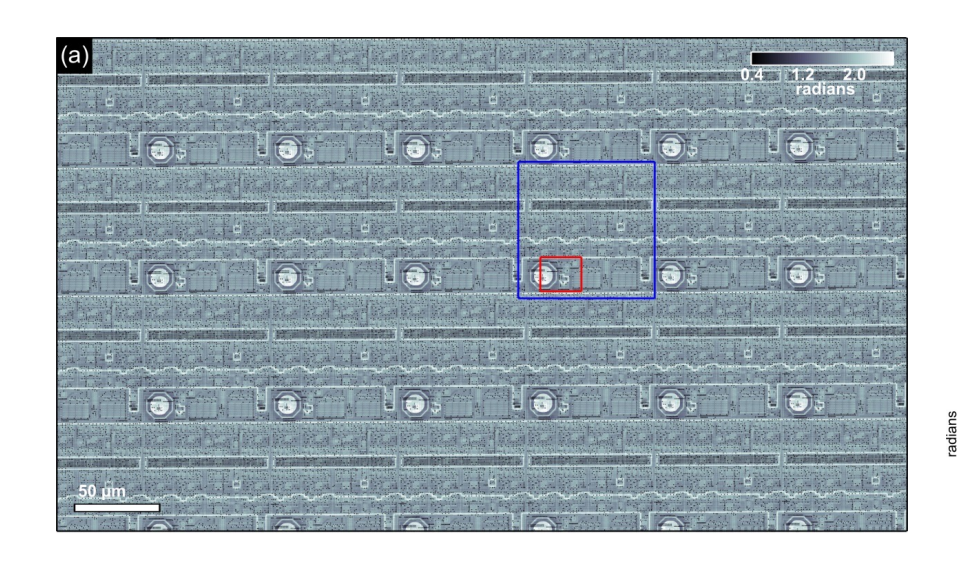


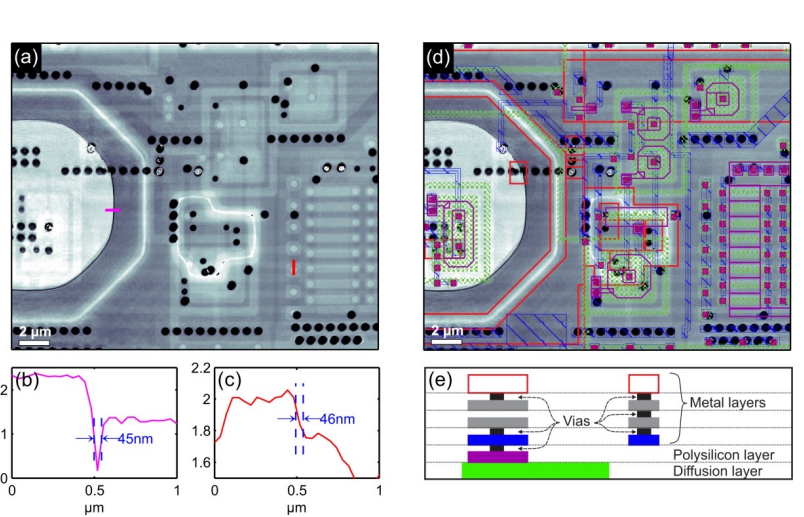


Imaging throughput – The Eiger self portrait

98.4 Mpixel (13,028 x 7,556)
Resolution 41 nm, 38.4 nm pixel
> 25,000 resolution elements / second
40 microsecond per resolution element







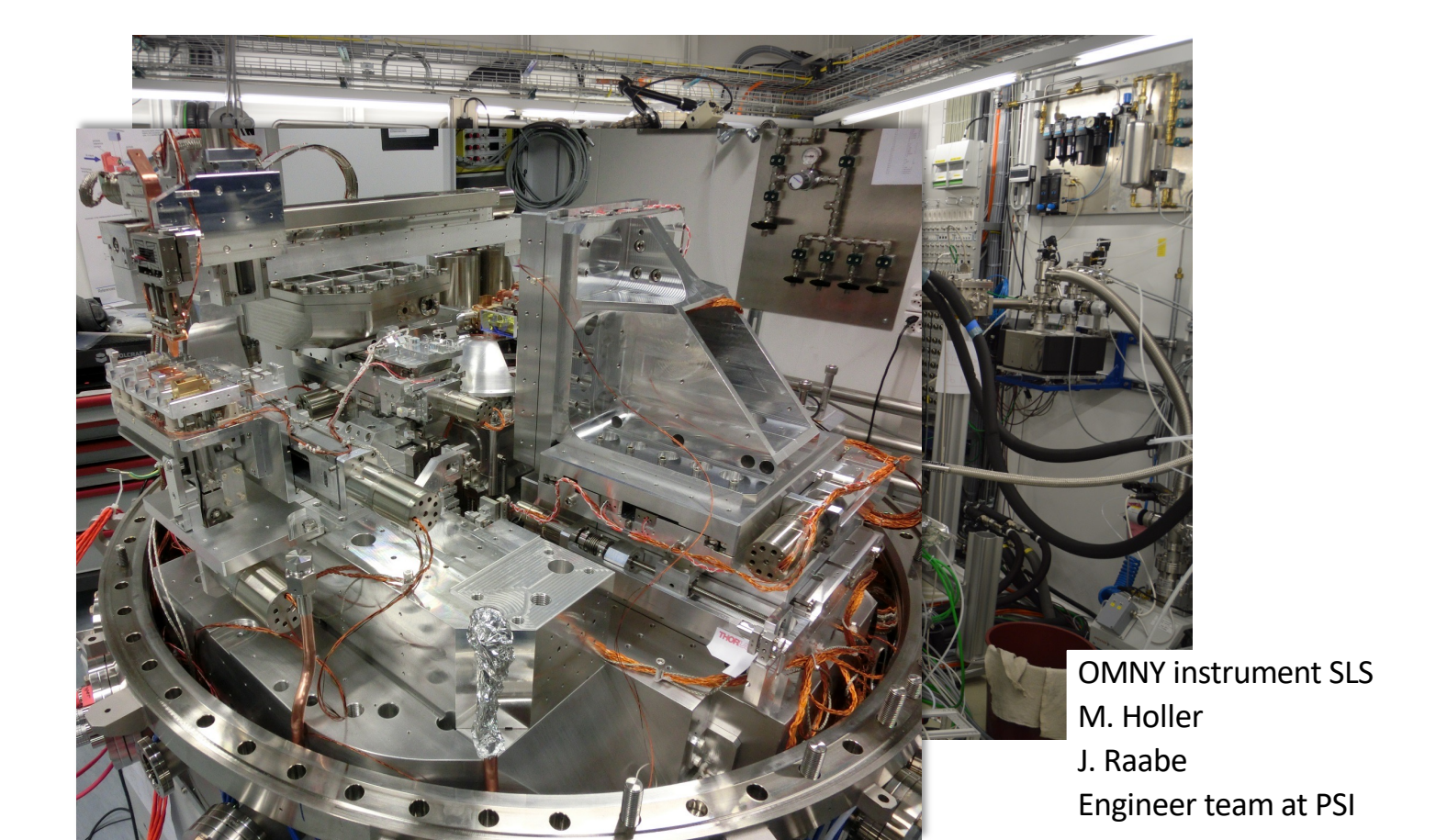


Ptychography

- X-ray ptychography is a robust, top-quality imaging technique:
 - very high phase sensitivity
 - quantitative phase and absorption contrast
 - very high spatial resolution
- allows for extended samples (compared to CDI)
- The illumination is separated from the complex-valued transmissivity of the sample and it does not need to be a plane wave
- Requires a stable illumination and position accuracy between illumination and sample equal or better than the aimed resolution
- Practical consequences: sophisticated instrumentation, especially for 3D
- Ptychography is performed nowadays in many 3rd generation synchrotron sources worldwide and its performance is expected to be much better in 4th generation sources..



Ptychography: accurate position control



EPFL PAUL SCHERRER INSTPITYCHOgraphy at cryogenic temperature

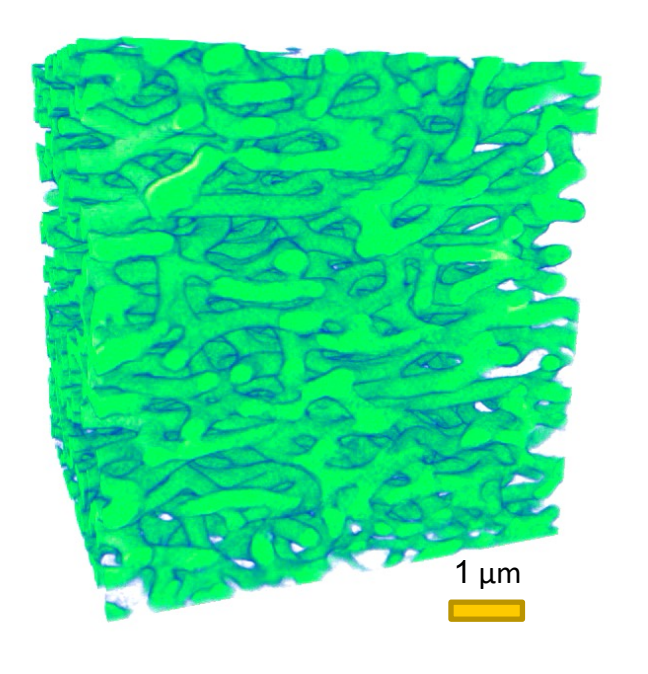


Cyphochilus

Radiation sensitive biological structure – Not measurable under non-cryogenic conditions.

Measured at 92K +/- 0.4 mK

Holler, M. et al. Review of Scientific Instruments **89**, 043706, (2018).

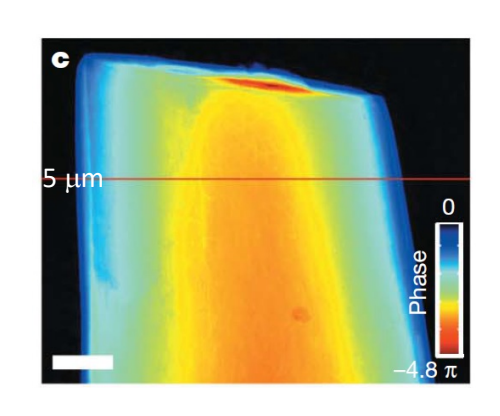


Bodo D. Wilts, et al Advanced Materials



Ptychography:

Quantitative mass density values



phase shift:

$$\phi(x,y) = -\frac{2\pi}{\lambda} \int \delta(\mathbf{r}) dz$$

electron density:
$$n_{\rm e}({\bf r})=rac{2\pi\,\delta({\bf r})}{\lambda^2 r_0}$$
 away from absorption edges!

mass density:
$$\rho = \frac{n_e A}{N_A Z}$$

with A: molecular mass

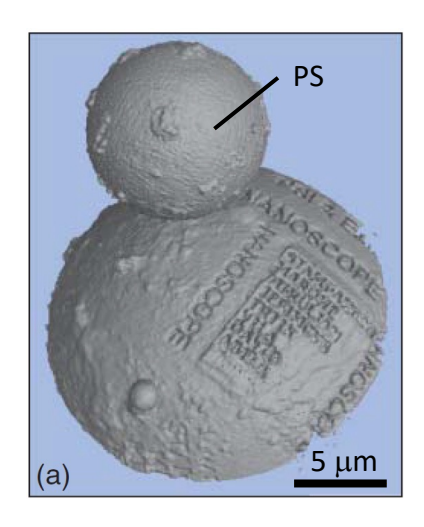
Z: number of electrons in the molecule



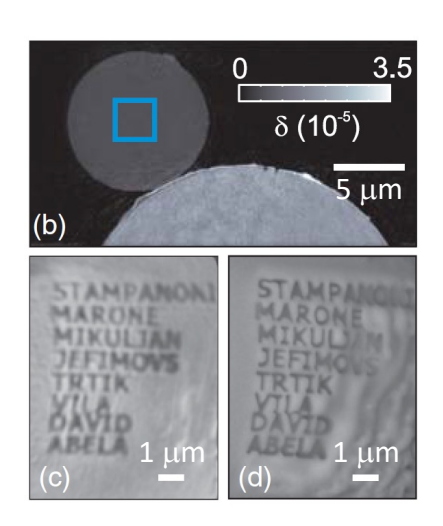
Ptychography: Quantitative mass density values

Demonstration of absolute density measurement

A. Diaz et al., Phys. Rev. B 85 (2012) 020104(R)



- Ptychographic tomography on test specimen
- Polystyrene sphere (PS) of 10 μm diameter with homogeneous density of 1.055 g/cm³

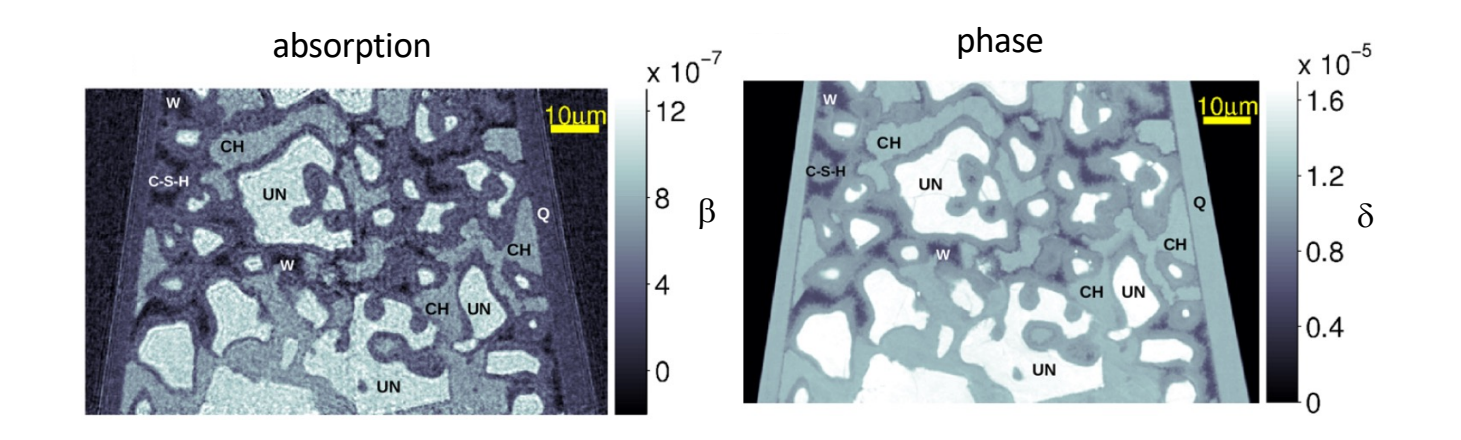


- Measured density on PS based on gray values: 1.048 ± 0.008 g/cm³
- (c) Spherical tomogram section
- (d) SEM image of the surface

Ana Diaz, PSI



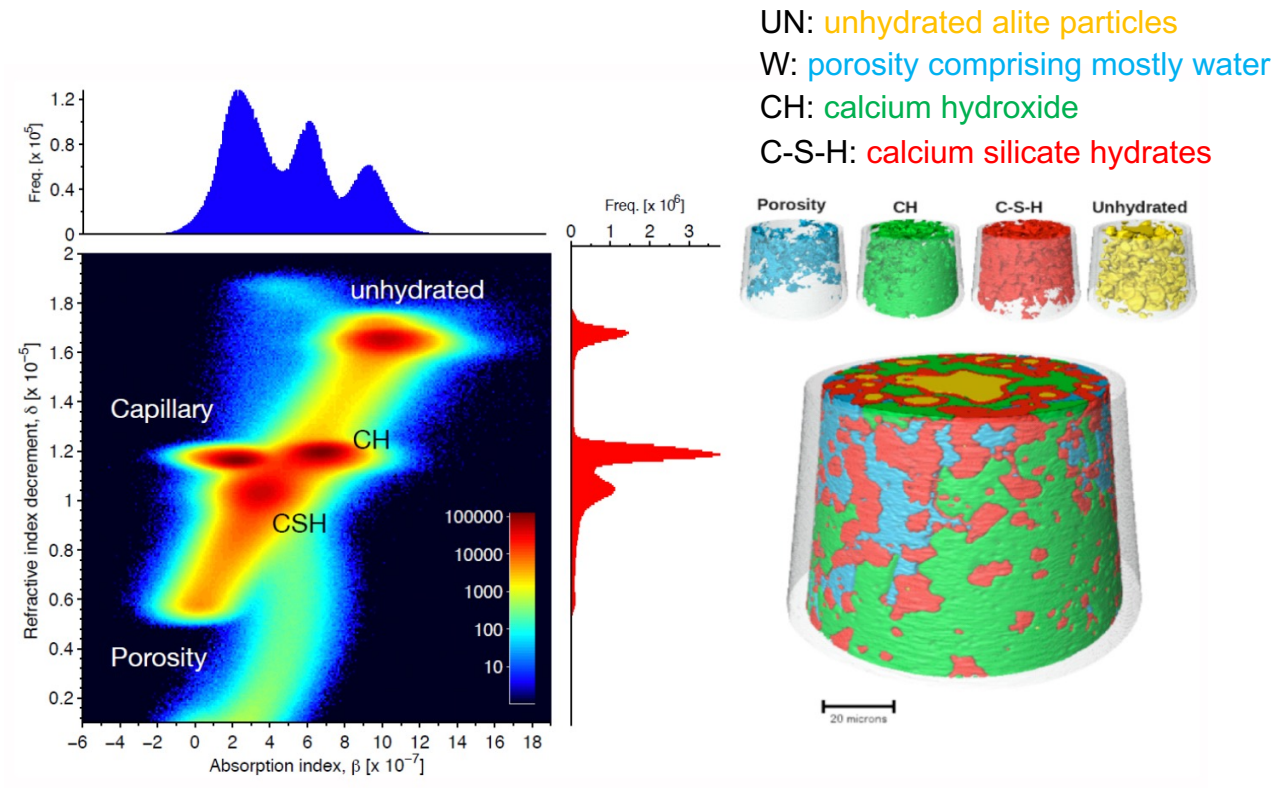
Ptychography on hydrated cement paste





Ptychography on hydrated cement – segmentation

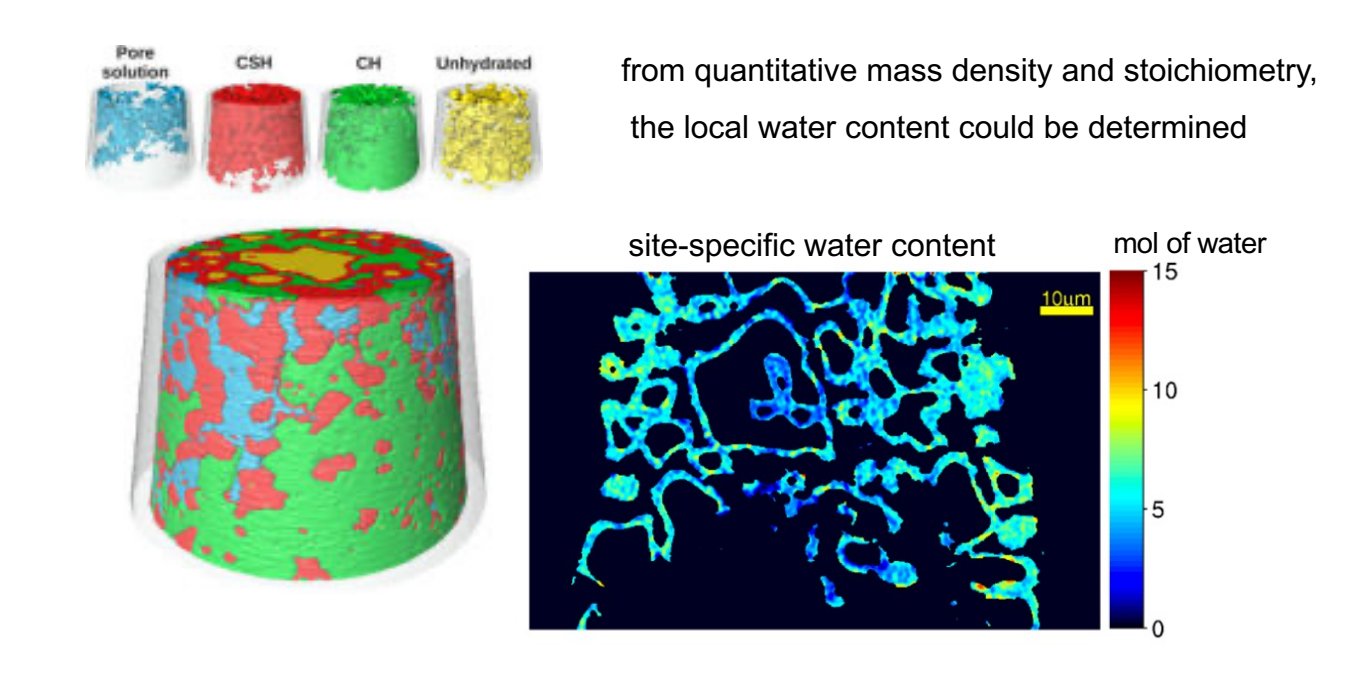
bivariate histogram of absorption and phase information for segmentation



da Silva J, et al. Langmuir 31, 3779 (2015).



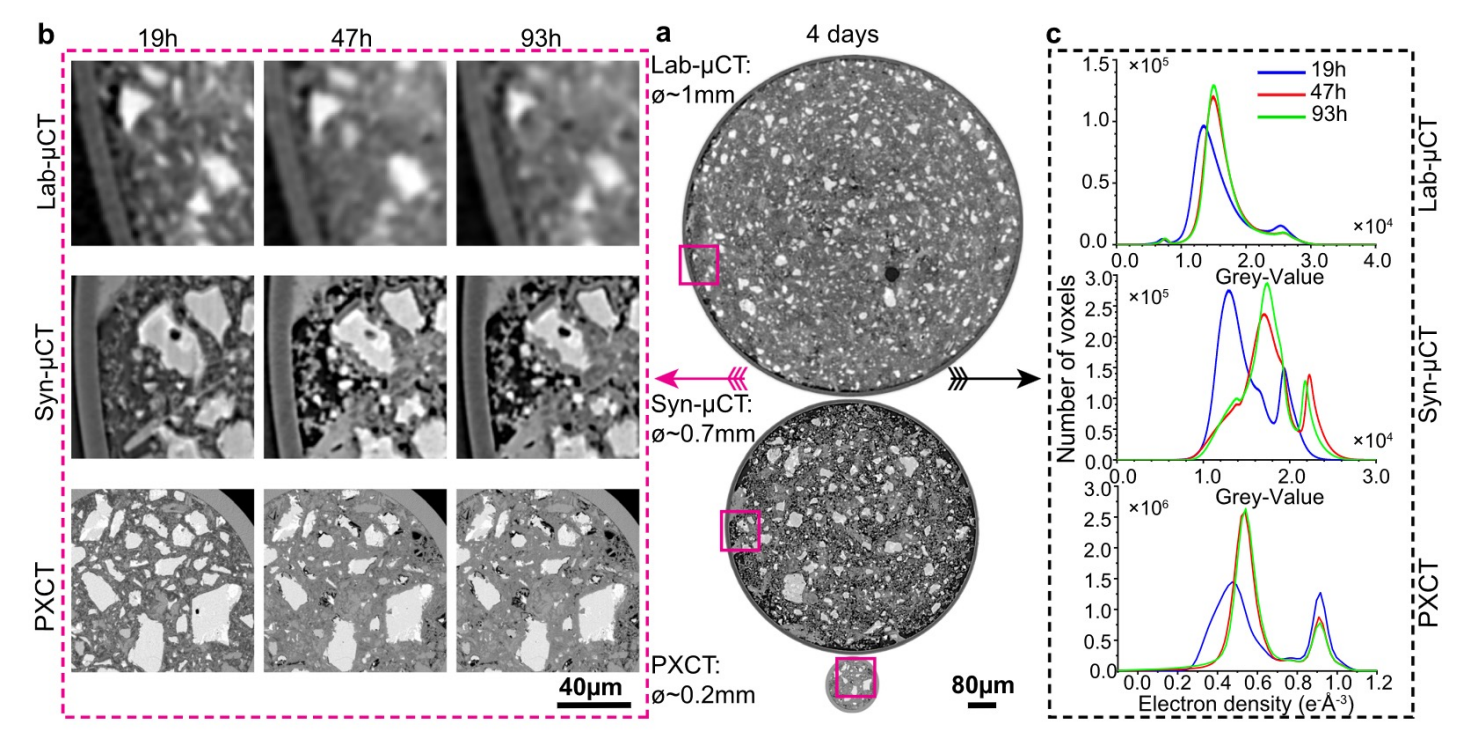
Ptychography on hydrated cement – water content



da Silva J, et al. *Langmuir* **31**, 3779 (2015).



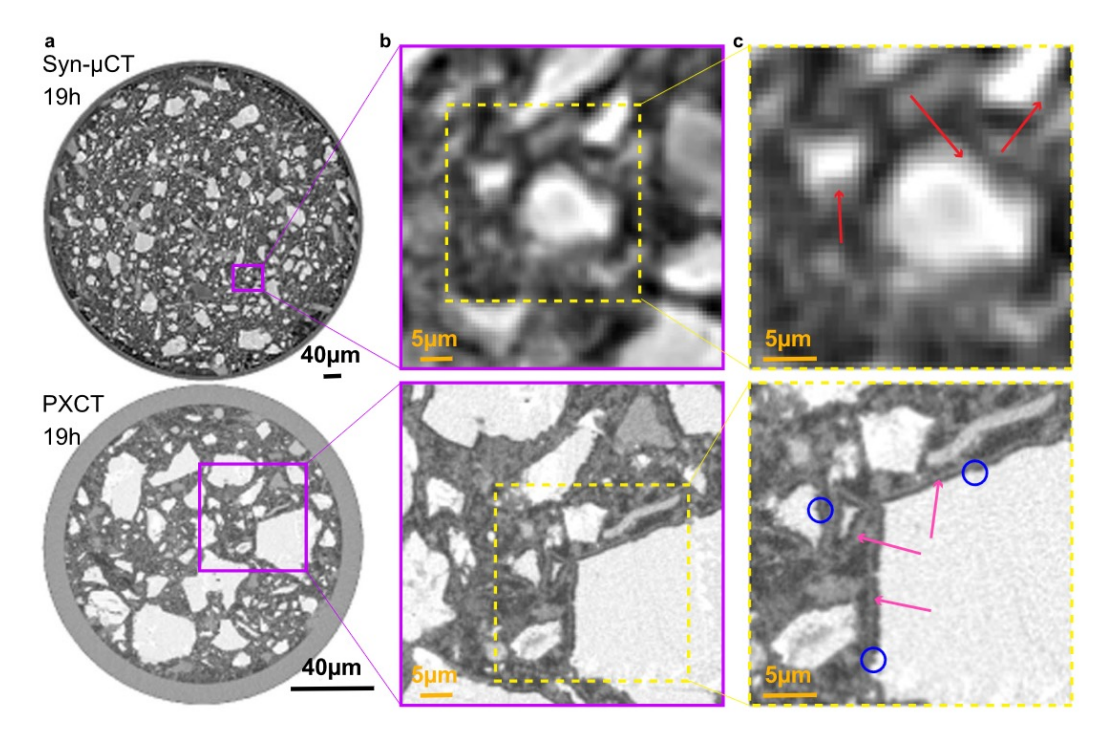
Laboratory/Synchrotron µCT and Ptychography on cement



Shirani, S., et al. (2023). Nature communications https://doi.org/10.1038/s41467-023-38380-1



Laboratory/Synchrotron µCT and Ptychography on cement

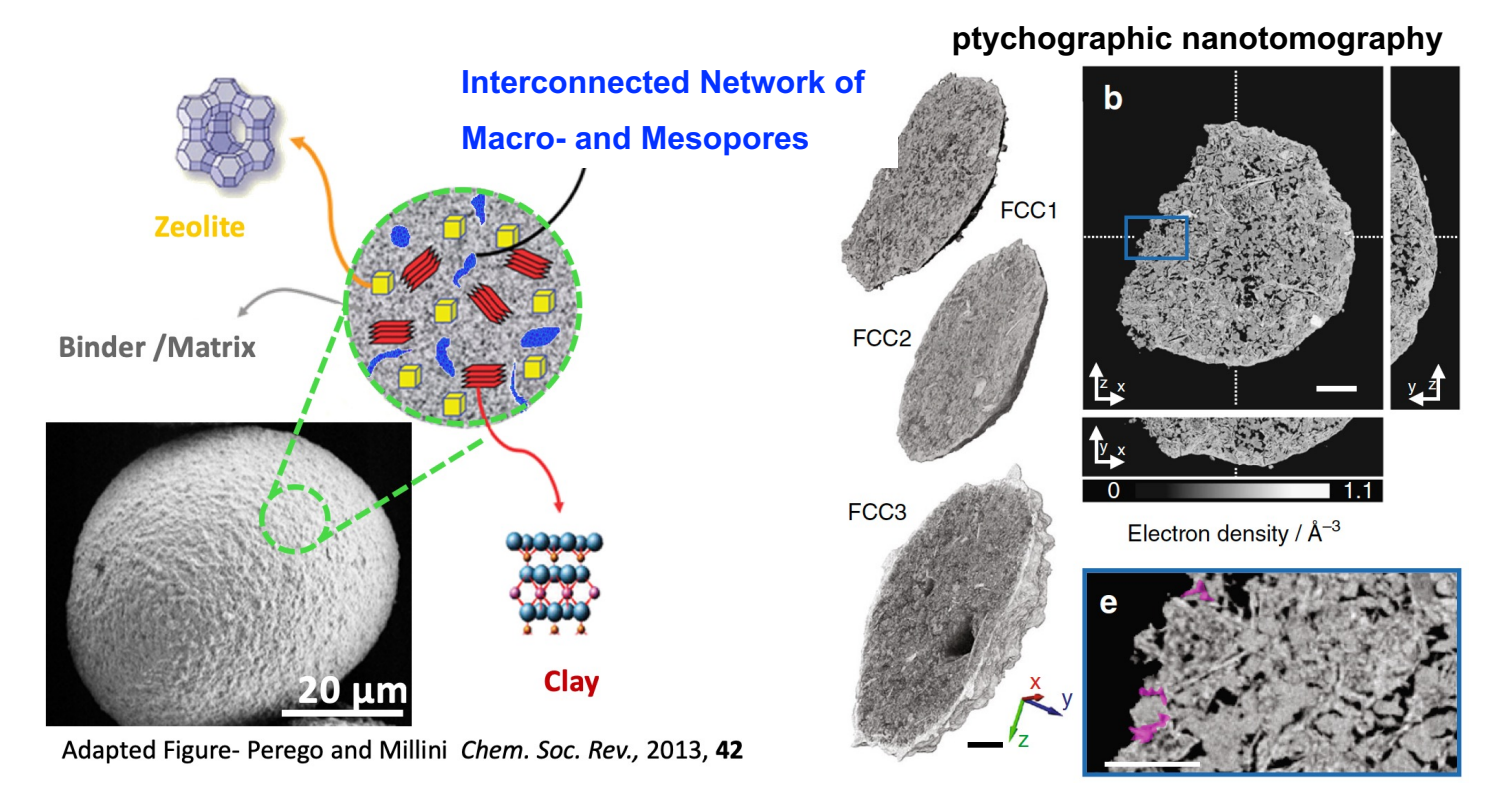


high resolution and contrast allows t resolve the C-S-H gel shells surrounding the alite particles (pink arrows) which is important to understand the mechanisms of cement hydration

Shirani, S., et al. (2023). Nature communications https://doi.org/10.1038/s41467-023-38380-1



Ptychography on catalytic particles

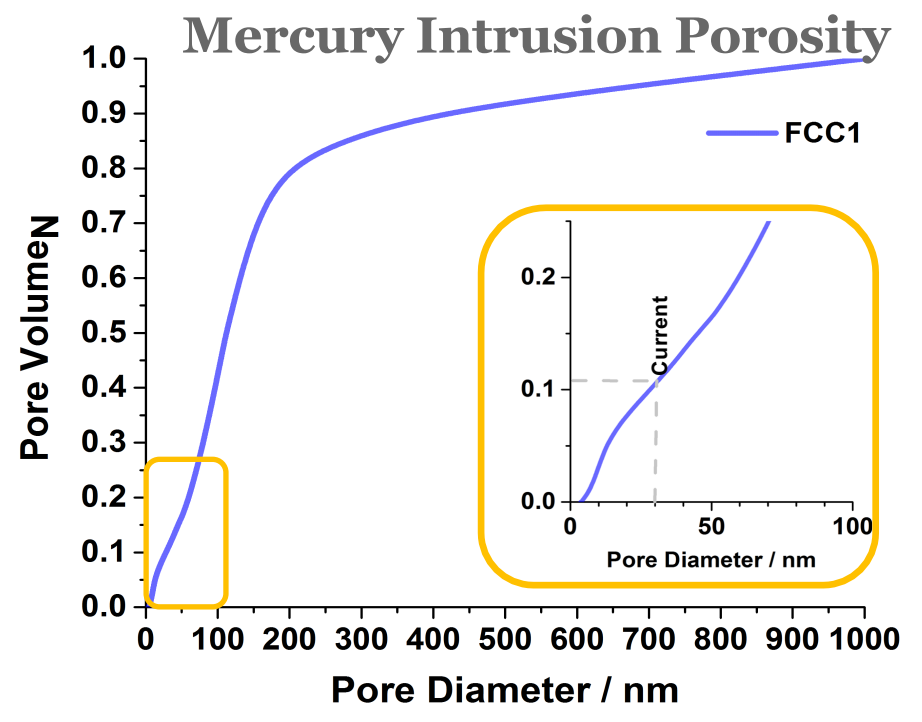


J. Ihli et al. Nature Communication, 2017, 8, 809



Ptychography – resolution vs. pore size

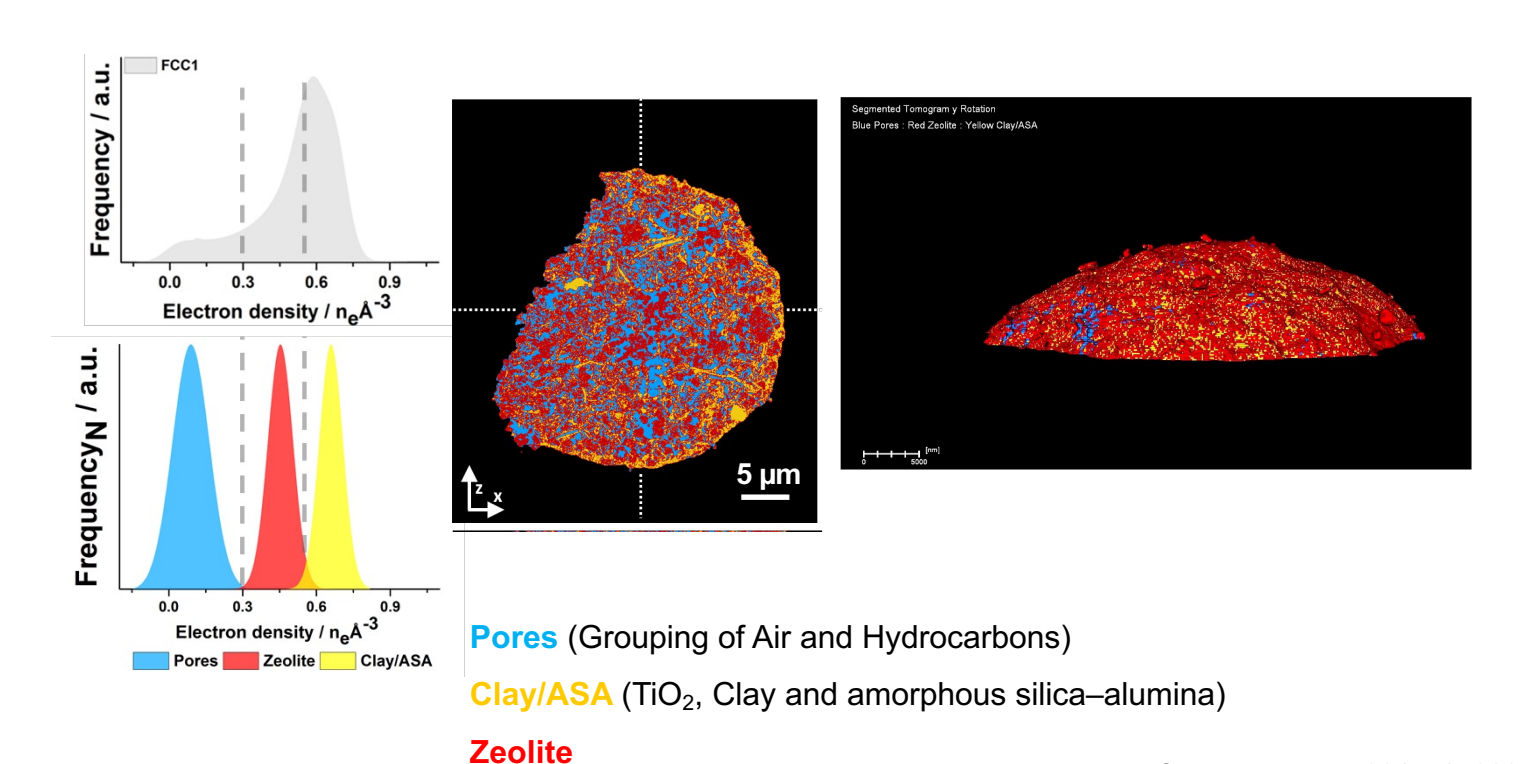
Resolution by Fourier shell correlations 31 nm



=> Tomograms probe a pessimistic ~90% of the macro and mesopore volume.



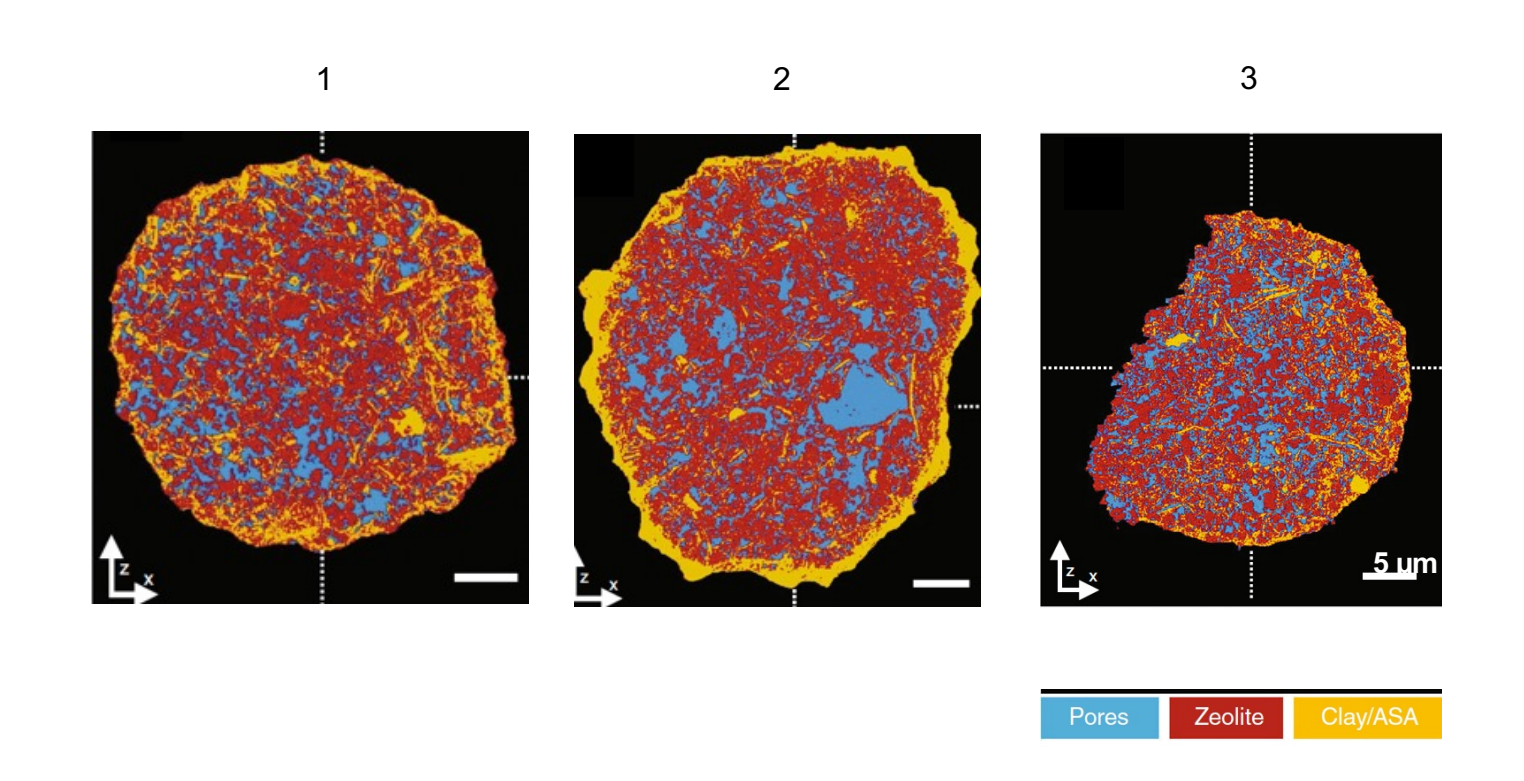
Ptychography on catalytic particle – component segmentation



J. Ihli et al. Nature Communication, 2017, 8, 809

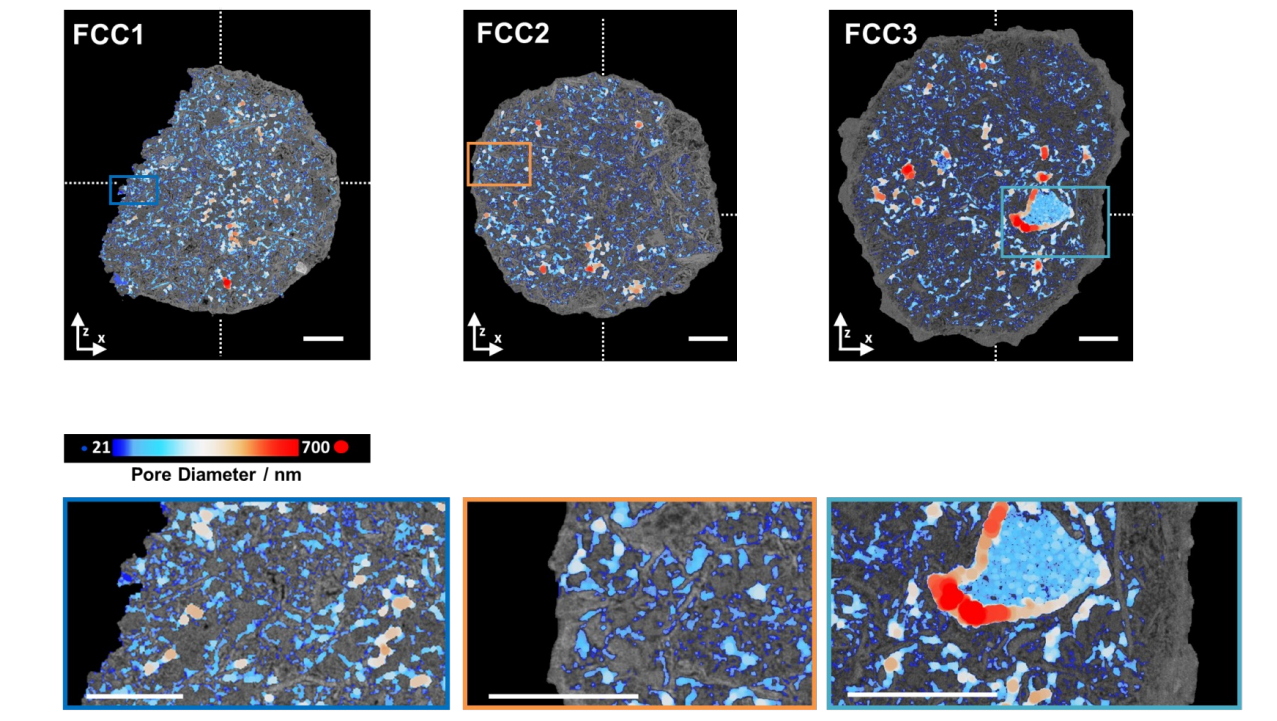


Which particle is the most deactivated?





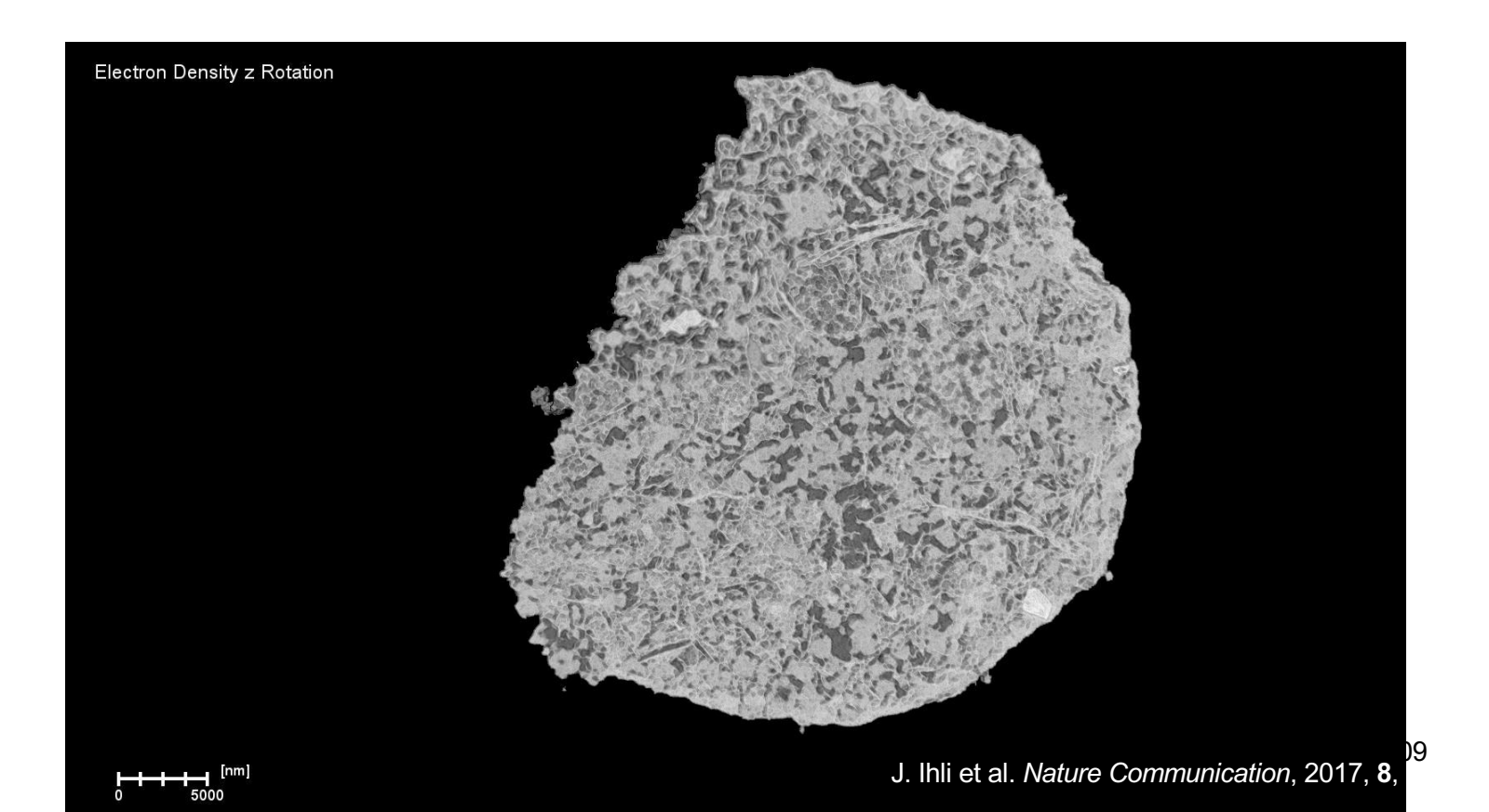
Ptychography on catalytic particle – pore size analysis



each porous region is fitted with maximal spheres filling this region best

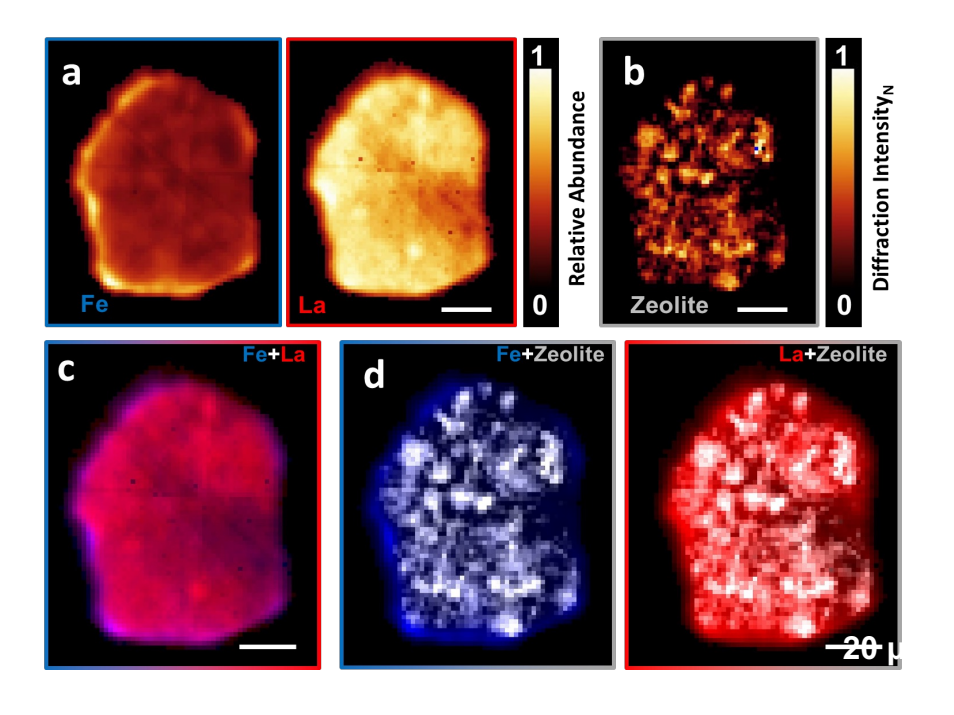


Ptychography on catalytic particle – pore size analysis and diffusion highways





XRD/XRF Tomography – on catalytic particle



- Iron representative of amorphous silicia-aluminia shell
- Lanthanum representative of zeolites in pristine state (look into past)
- XRD current location of crystalline components

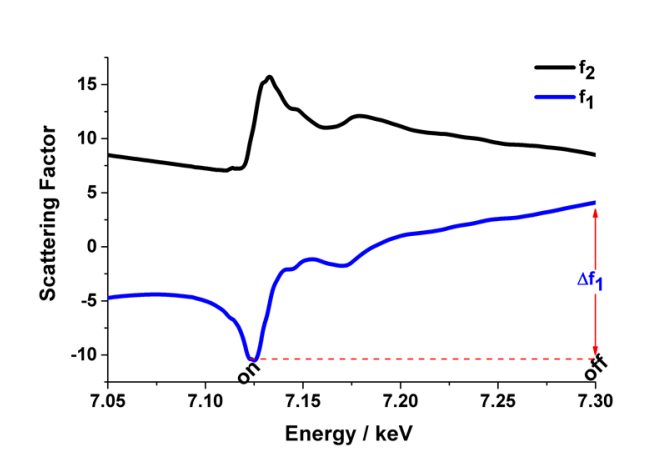


Resonant Ptychographic Tomography

3D quantitative colocalization of chemical elements with physical features of functional matter with nanoscopic resolution.

Here colocalization of iron impurities within the primary components of a deactivated FCC catalyst. Spatial Resolution \sim 39 nm.

Acquired by means of a comparison of *on* and *off* resonance Fe-K edge ptychographic tomograms.



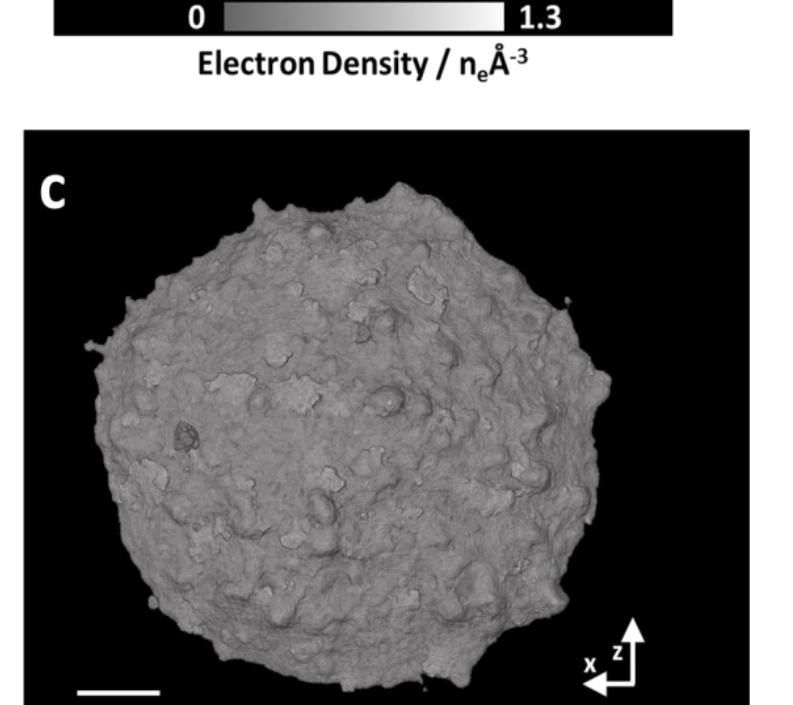
7112 7118 7120 7122 7124 7126 7112 7118 7120 7122 7124 7126

~ 95% of iron species in question posses a resonant energy of +- 2eV of the selected on-resonance energy!

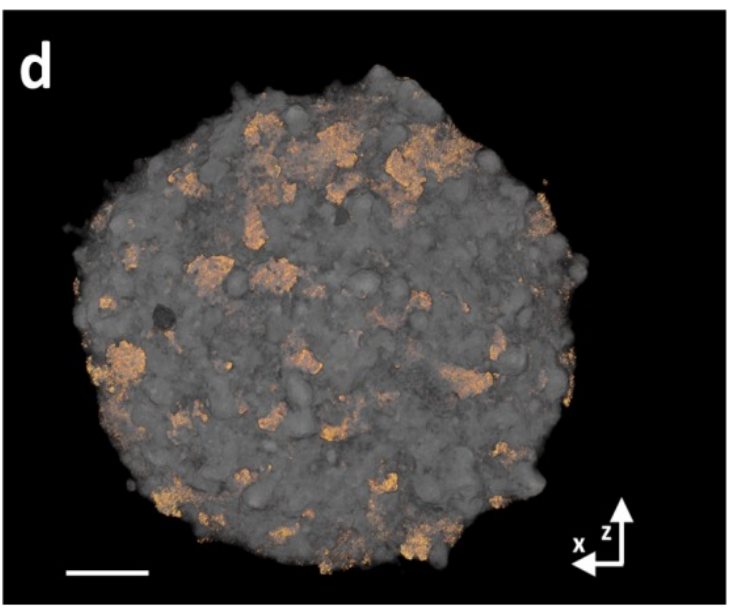


Resonant Fe *K*-Edge Ptychographic Tomography

Deactivated Fluid Catalytic Cracking Catalyst (FCC3) measured electron density tomogram and iron distribution



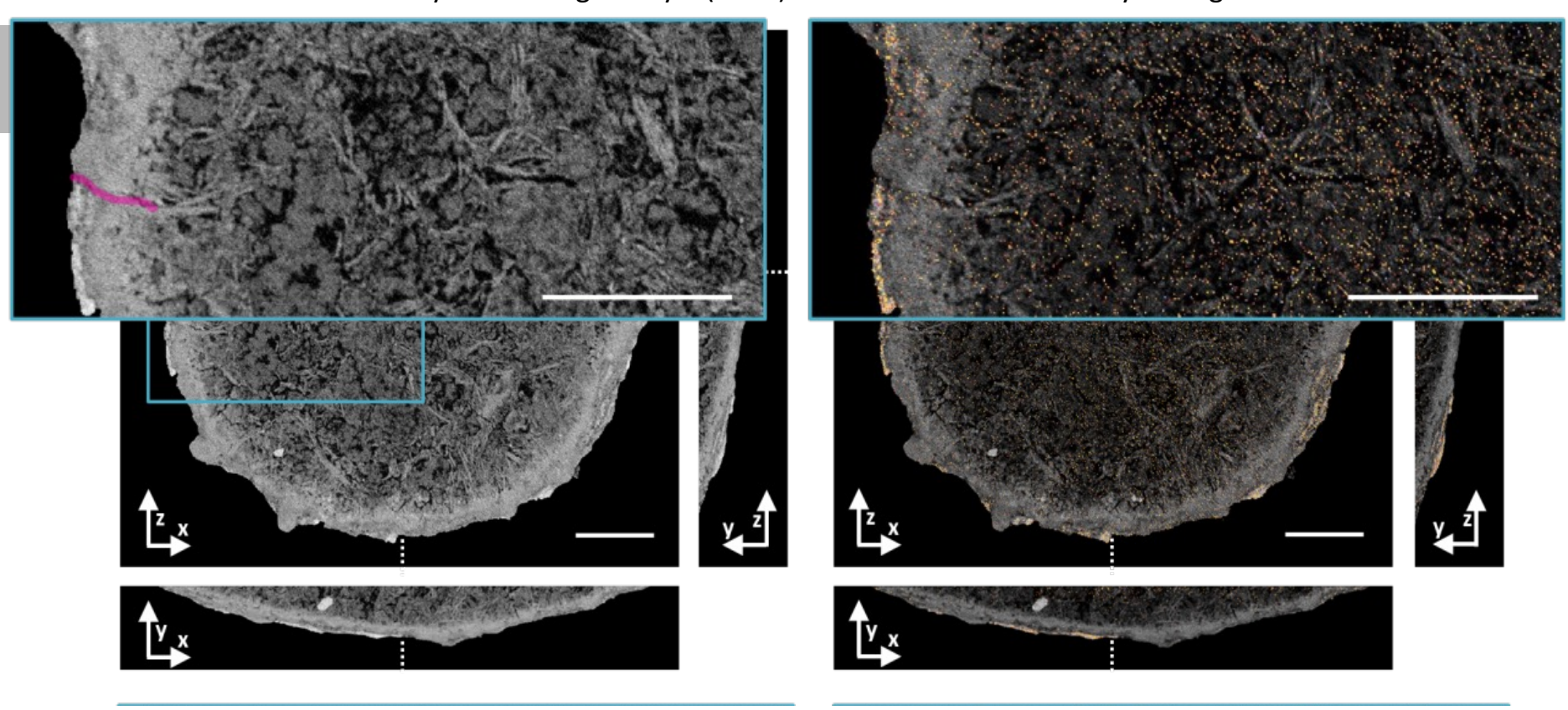






Resonant Fe *K*-Edge Ptychographic Tomography

Deactivated Fluid Catalytic Cracking Catalyst (FCC3) measured electron density tomogram and iron distribution





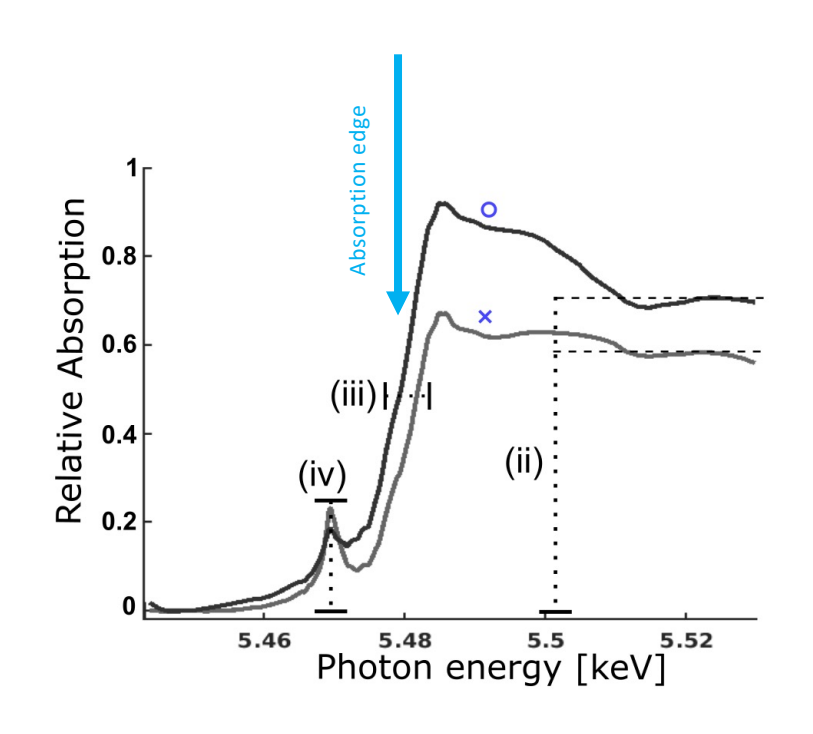
Combining Ptychography with XANES

Example spectra across vanadium K-edge

Chemical information

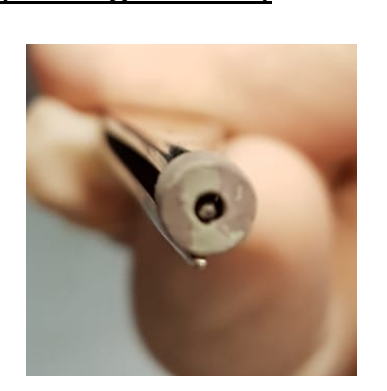
- (ii) Vanadium concentration
- (iii) Oxidation state
- (iv) Coordination geometry (local crystalline order)

Combine with ptychotomo to obtain 3D nanoscale maps of chemical composition.





Vanadium phosphorus oxides catalyst
Used in butane oxidation as prerequisite for household and industrial plastics (biodegradable)



10 micron diameter pillars



Chemical information, such as oxidation state can be obtained by measuring the X-ray transmission spectra

Combine with ptychotomo to obtain 3D nanoscale maps of chemical composition

Measuring one full tomogram per energy would be too slow

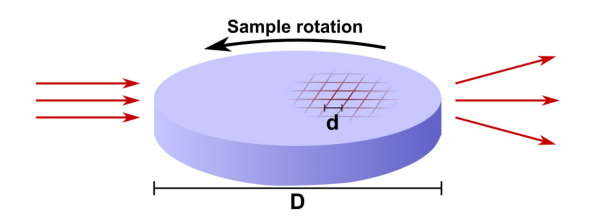
Gao et al, "Sparse ab initio x-ray transmission spectrotomography for nanoscopic compositional analysis of functional materials", Sci. Adv. 7, eabf6971 (2021)

Manuel Guizar-Sicairos, EPFL/PSI



Sparse measurements

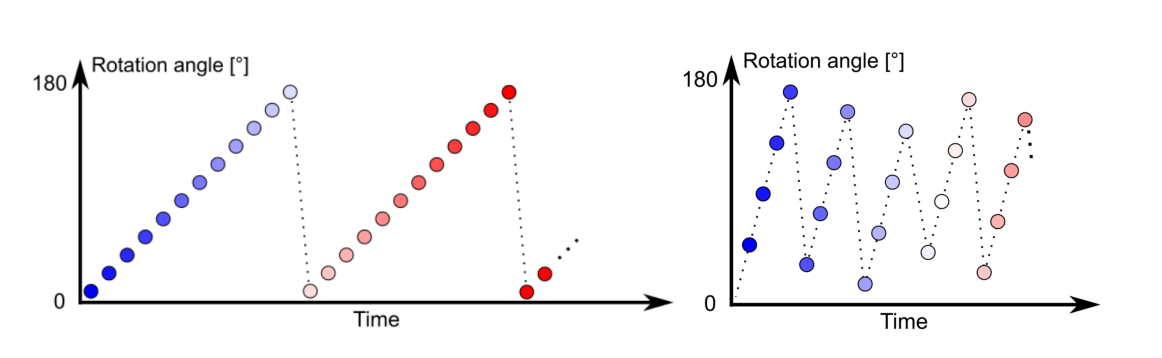
<u>Number of projections</u> needed in a <u>tomography measurement</u> is given by the *Crowther Criterion*:

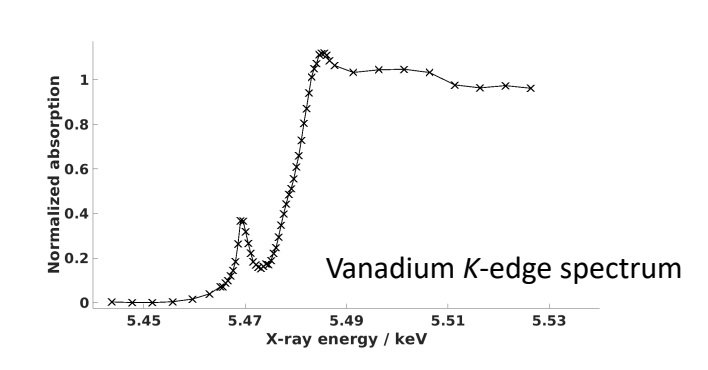


$$n_p = \frac{\pi D}{2d_{(half-period)}}$$

Conventional sampling of a <u>full tomogram at each time frame / X-ray energy</u> is too long, and not necessary

Information is sparse in multidimensional space

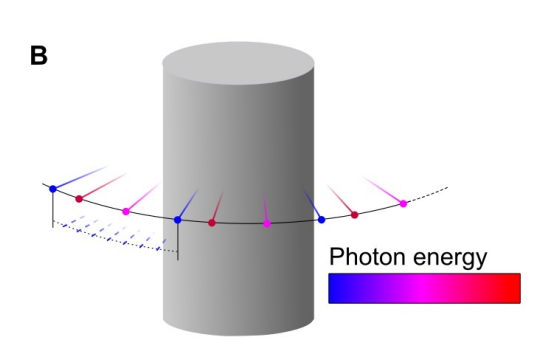


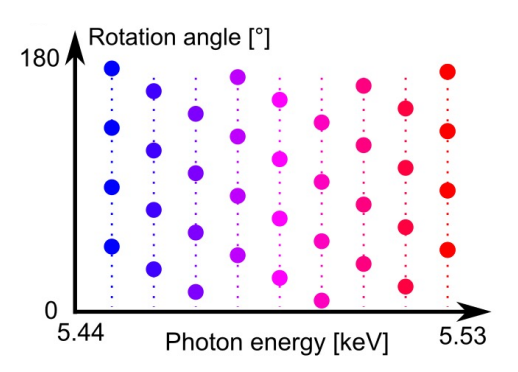




Crucial to reconstruct hyperspectral volume from all projections simultaneously

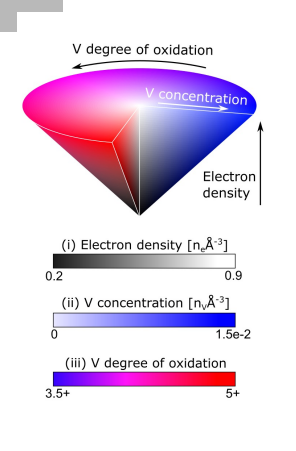
- Measured at 60 energies between 5.443-5.465 keV, minimum step 0.5 eV
- Sparse angular sampling, <u>11%</u> of Crowther sampling criteria. About 1 day of measurement per sample.
- Leverage signal sparsity in the spectral dimension → Only a few spectral modes actually exist
- Novel iterative method for <u>ab initio</u> reconstruction. Combination of PCA and SART. Preserves resolution, quality and SNR



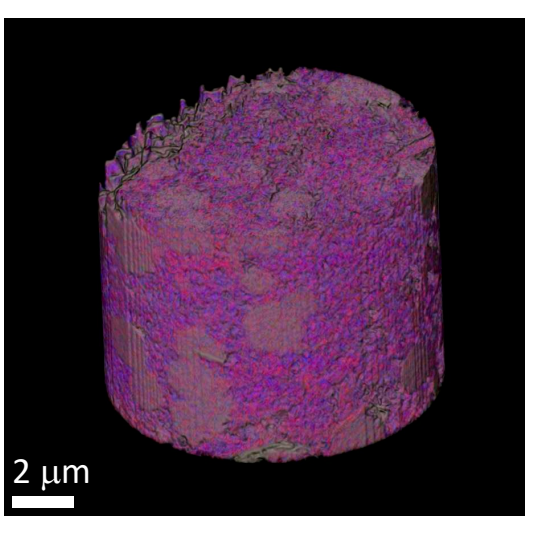


Gao et al, "Sparse ab initio x-ray transmission spectrotomography for nanoscopic compositional analysis of functional materials", Sci. Adv. 7, eabf6971 (2021)

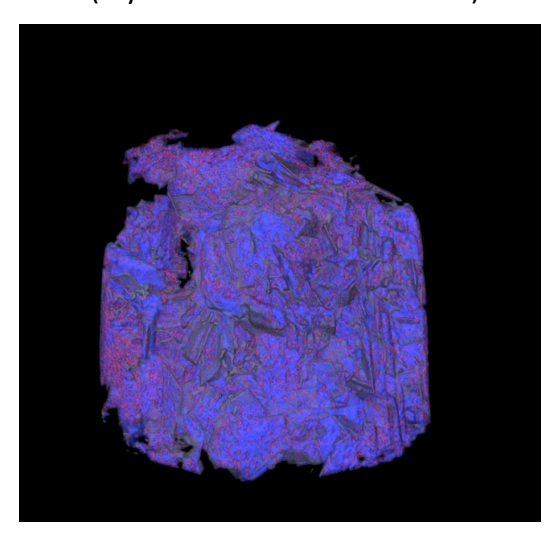




Pristine

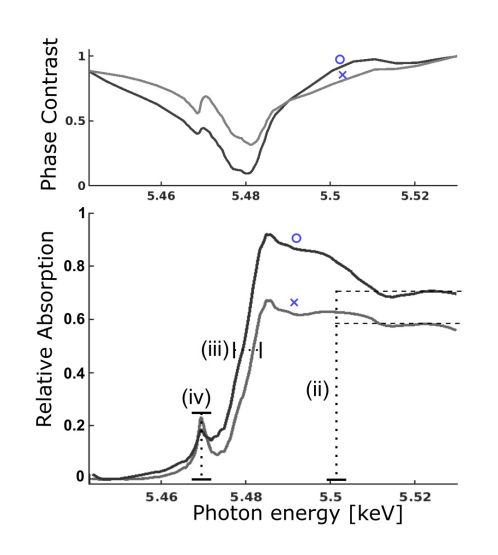


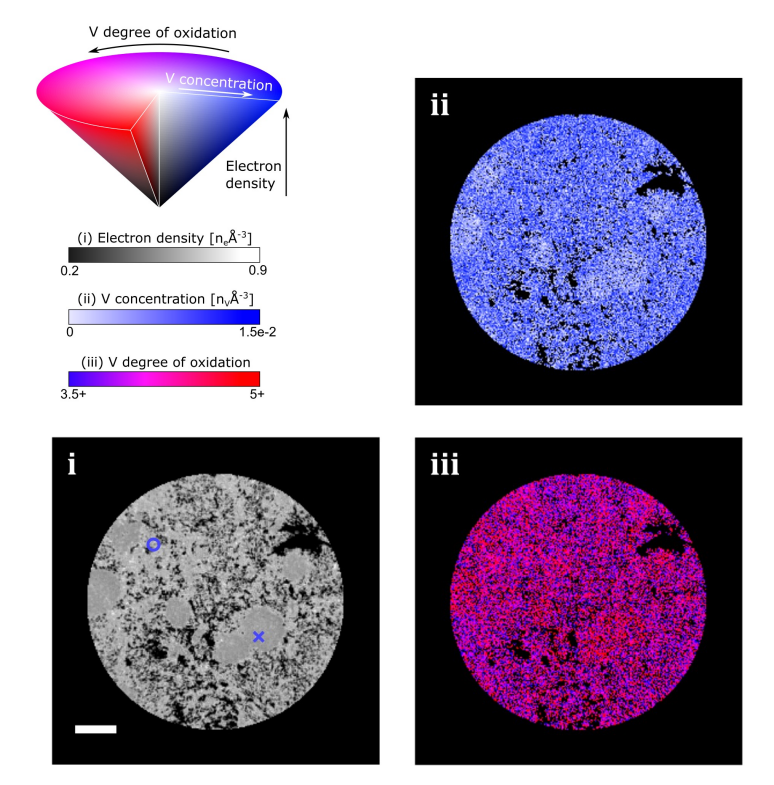
Used (4 years in industrial reactor)



Hyperspectral tomogram resolution 26 nm







Gao et al, "Sparse ab initio x-ray transmission spectrotomography for nanoscopic compositional analysis of functional materials", Sci. Adv. 7, eabf6971 (2021)



3D nanoscale maps of defects

Further analysis reveals <u>crystal structure defects</u> (vanadyl deficiencies) in the surface regions of the used catalyst sample. Thus far only theorized to exist as a possible active sites in the catalyzed reaction

